Computation for Epidemic Prediction with Graph Neural Network by Model Hybridization

Xiangxin Kong¹, Hang Wang², Yutong Li³, Yanghao Chen⁴, and Zudi Lu^{5,*}

¹Department of Biostatistics, City University of Hong Kong; xikong9-c@my.cityu.edu.hk ²Department of Biostatistics, City University of Hong Kong; hwang858-c@my.cityu.edu.hk ³Department of Biostatistics, City University of Hong Kong; yli2487-c@my.cityu.edu.hk ⁴Department of Biostatistics, City University of Hong Kong; yanghchen5-c@my.cityu.edu.hk ⁵Department of Biostatistics, City University of Hong Kong; Correspondence: zudilu@cityu.edu.hk

Abstract

Modelling epidemic events such as COVID-19 cases in both time and space dimensions is an important but challenging task. Building on in-depth review and assessment of two popular graph neural network (GNN)-based regional epidemic forecasting models of EpiGNN and ColaGNN, we propose a novel hybrid graph neural network model, EpiHybridGNN, which integrates the strengths of both EpiGNN and ColaGNN. In the EpiGNN, through its transmission risk encoding module and Region-Aware Graph Learner (RAGL), both multi-scale convolutions and Graph Convolutional Networks (GCNs) are combined, aiming to effectively capture spatio-temporal propagation dynamics between regions and support the integration of external resources to enhance forecasting performance. While, in the ColaGNN, a cross-location attention mechanism, multi-scale dilated convolutions, and graph message passing are utilized to address the challenges of long-term forecasting through dynamic graph structures and spatio-temporal feature fusion. Both enjoy respective advantages but also share mutual shortcomings. Our EpiHybridGNN is therefore designed to combine the advantages of both EpiGNN, in its risk encoding and RAGL, and ColaGNN, in its long-term forecasting capabilities and dynamic attention mechanisms. This helps to form a more comprehensive and robust prediction of spatio-temporal epidemic propagation. The computational architecture, core formulas and their interpretations of our proposed EpiHybridGNN are provided. Multiple numerical real data experiments validate that our EpiHybridGNN significantly outperforms both EpiGNN and ColaGNN in epidemic forecasting with comprehensive insights and references offered.

Keywords: Epidemic Forecasting; HybridGNN; Spatial-temporal dependence

1 Introduction

The global spread of epidemics poses a significant threat to public health. Accurate epidemic forecasting is crucial for effective disease control, optimizing medical resource allocation, and promoting drug development. Traditional models[1, 2, 3], due to overly simplistic assumptions, struggle to capture complex non-linear spatio-temporal relationships. In recent years, deep learning, especially Graph Neural Networks (GNNs)[4, 5], has emerged as a vital tool for epidemic forecasting due to its powerful ability to process non-Euclidean structured data and capture complex correlations between nodes.

It is against this backdrop that EpiGNN and ColaGNN emerged as innovative GNN models. EpiGNN focuses on integrating transmission risk (including local and global transmission

risk) and geographical information, emphasizing explicit modeling of local and global propagation mechanisms. Through its Region-Aware Graph Learner (RAGL) and multi-scale convolutions, it supports external resource integration to enhance forecasting performance. ColaGNN, conversely, emphasizes long-term forecasting through a cross-location attention mechanism and multi-scale dilated convolutions, excelling at capturing complex dynamic dependencies of non-adjacent regions, particularly in long-term predictions.

Despite their individual strengths in specific scenarios, EpiGNN and ColaGNN exhibit significant complementarity. EpiGNN excels in external data integration and handling early and mid-term changes, but its graph construction mechanism limits its long-term forecasting ability. ColaGNN performs outstandingly in long-term forecasting but may lack explicit risk encoding.

This paper aims to provide an in-depth analysis and comparison of EpiGNN and ColaGNN, and building on this, proposes a novel hybrid model named HybridGNN (EpiCola-GNN). HybridGNN stands out with its innovative modular architecture, designed to excel in modeling both short-term and long-term disease propagation patterns. The model begins with a Temporal Feature Extraction module, inspired by ColaGNN, which employs multi-scale 1D convolutions to extract short- and long-term temporal features. This is complemented by a Transmission Risk Encoding module, drawing from EpiGNN, which computes local risk using geographic degree information and global risk via temporal features. A key highlight is the Dynamic Graph Construction module, which fuses ColaGNN's RNN-based attention mechanism with EpiGNN's geographic and external relation priors to generate a dynamic adjacency matrix. This dynamic framework supports a Feature Fusion and Graph Message Passing process through multi-layer GCNs, where initial node features are propagated and enriched with residual connections. Finally, the Prediction module concatenates GCN outputs with RNN hidden states, optionally incorporating a residual window to yield the final prediction. By leveraging ColaGNN's efficient stable long-term forecasting performance with EpiGNN's short-term dynamic modeling, HybridGNN achieves a balanced approach that excels in capturing rapid outbreaks as well as prolonged epidemic trends. This dual-focus capability, combined with its scalability, positions HybridGNN as a powerful tool for epidemic forecasting.

The remainder of this paper is organized as follows. This paper begins by reviewing related work in Section 2, followed by a detailed description of the EpiGNN and ColaGNN architectures in Section 3. Section 4 presents the experimental analysis of the two models. Based on the comparative advantages and disadvantages discussed in Section 5, we propose HybridGNN in Section 6 to enhance performance across multiple datasets. Then we analyze the strengths of the proposed HybridGNN framework and discuss potential directions for further improvement in Section 7. Finally, conclusions are drawn in Section 8.

2 Related Work

In the field of epidemic forecasting, recent studies have increasingly leveraged deep learning models. For instance, research by [6, 7] specifically explored models for direct long-term epidemiological predictions, achieving good results. Wu et al. [7] proposed CNNRNN-Res, a model combining CNN and RNN. DEFSI [8] integrated deep neural network methods with causal models. Jung et al. [9] designed a self-attention-based method for regional influenza forecasting.

GNNs have shown prominent performance in epidemic forecasting due to their ability to capture inter-node correlations in graph structures. For example, STGCN [10] is a deep learning model specifically designed to process data with spatial and temporal dependencies. It combines Graph Convolutional Networks (GCNs) [11, 12] with traditional sequence models (such as convolutional sequence learning or recurrent neural networks) to simultaneously capture spatial

and temporal features in the data. However, existing GNN methods face two major challenges: accurately capturing potential propagation relationships between regions and effectively utilizing regional propagation risk information. Both EpiGNN and ColaGNN address these challenges effectively through innovative module designs. Through the Region-Aware Graph Learner (RAGL), EpiGNN [13] can dynamically learn and fuse temporal correlations, geographical priors, and external resources to construct an adaptive propagation graph structure. This enables flexible capture of complex and evolving propagation paths. It extracts multi-scale temporal features via Multi-Scale Convolutions, and combines them with Local Transmission Risk Encoding and Global Transmission Risk Encoding to comprehensively encode a region's potential propagation risk. With powerful dynamic graph learning capabilities, EpiGNN is highly effective at capturing rapidly evolving, non-fixed propagation relationships in the short term, but potentially leading to relative deficiencies in modeling long-term, stable temporal dependencies. Through its Loc-Aware Attention, ColaGNN [14] dynamically calculates and adjusts edge weights between regions on top of a pre-defined base graph structure using an attention mechanism. This allows for more adaptive information propagation and the measurement of influence between non-adjacent regions. The combination of RNN and Dilated Conv modules makes it highly effective at capturing long-term, complex temporal patterns. Despite introducing dynamic edge weights, ColaGNN's underlying graph topology fundamentally relies on pre-defined connections. For propagation events that change rapidly in the short term or completely break existing topological structures, its adaptability is less robust compared to EpiGNN. Therefore, to construct a more comprehensive and robust spatio-temporal forecasting model that can effectively address both short-term dynamics and long-term trends, it is necessary to build a HybridGNN.

3 Model Architecture

3.1 Problem Definition

We formulate epidemic forecasting as a graph-based spatiotemporal propagation problem. Let there be N locations. The historical case data is represented as $\mathbf{X} = [\mathbf{x}_1, \dots, \mathbf{x}_t]$, where each $\mathbf{x}_z \in \mathbb{R}^N$ denotes the case counts across all locations at time z. The goal is to predict future case counts \mathbf{x}_{t+h} , where h is the prediction horizon. We utilize a look-back window of size T, i.e., $[\mathbf{x}_{t-T+1}, \dots, \mathbf{x}_t] \in \mathbb{R}^{N \times T}$, as input. For each region i, the corresponding time series is denoted as $\mathbf{x}_{i:} = [x_{i,t-T+1}, \dots, x_{i,t}] \in \mathbb{R}^{1 \times T}$. In addition, we incorporate a static geographical adjacency matrix $\mathbf{A}^{\text{geo}} \in \mathbb{R}^{N \times N}$, where $a_{i,j}^{\text{geo}} = 1$ indicates that regions i and j are geographically connected.

3.2 EpiGNN Model Framework

EpiGNN is an epidemic forecasting framework that integrates spatio-temporal modeling to capture geographic and temporal patterns, with a learnable graph structure that dynamically infers transmission relationships. It takes historical regional case data through multi-scale convolutions for analyzing trends at different time spans, a transmission risk encoder incorporating mobility and environmental factors, RAGL, and GCN for propagation modeling [13]. Its process is as follows:

Multi-Scale Temporal Feature Extraction (Region-Aware Convolution)

This module extracts rich temporal features for each region i from its time series $\mathbf{x}_{i:} \in \mathbb{R}^{1 \times T}$ using a multi-branch convolutional structure. It consists of several parallel convolutional branches, each designed to capture distinct temporal patterns by employing specific combinations of kernel sizes and dilation rates. These branches are categorized as follows:

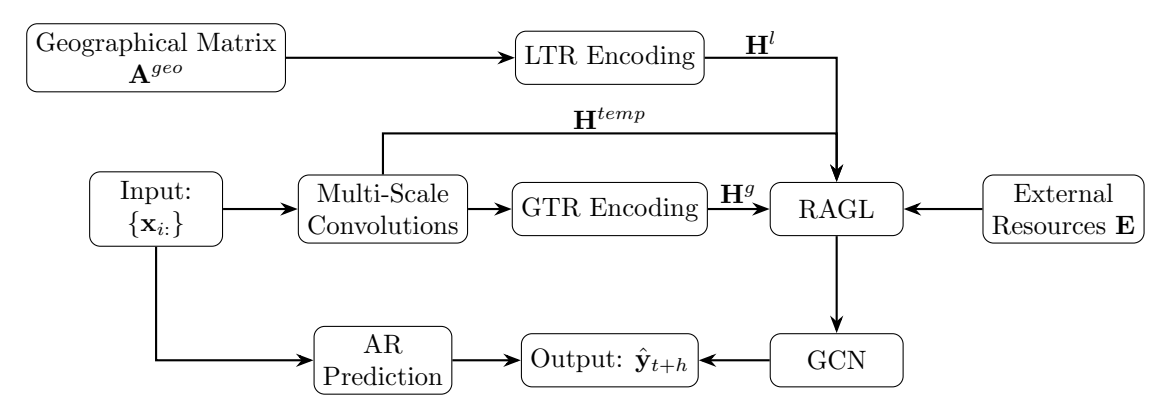


Figure 1: EpiGNN workflow

- Local Pattern Branches (M_L branches): These branches utilize relatively small kernel sizes s_l and a dilation rate of $r_l = 1$ to capture consecutive short-term dependencies.
- Periodic Pattern Branches (M_P branches): These branches also use relatively small kernel sizes s_p but employ larger dilation rates $r_p > 1$ to capture recurrent or periodic short-term trends that span across intervals.
- Global Pattern Branches (M_G branches): These branches employ a kernel size equal to the full time window length T (with a dilation rate of $r_g = 1$) to capture comprehensive, overarching patterns across the entire observation period.

The total number of branches is $M = M_L + M_P + M_G$. Each of the M branches employs k filters and all filters within a given branch use the same kernel size and dilation rate. For a convolutional filter $\mathbf{f}_{n,1\times s,r} \in \mathbb{R}^{1\times s}$ (where $n=1,\ldots,k$ is the filter index), it represents a kernel of size s applied along the temporal dimension, with a width of 1, and a temporal dilation rate r. The convolution operation at step j for location i is defined as:

$$(\mathbf{x}_{i:} \star \mathbf{f}_{n,1 \times s,r})[j] = \sum_{n=0}^{s-1} \mathbf{f}_{n,1 \times s,r}[0,p] \cdot \mathbf{x}_{i:}[j-r \times p]$$

$$\tag{1}$$

Here, \star is convolution operation. Let $\mathbf{X}_i^{(m)} \in \mathbb{R}^{k \times L_m}$ denote the output feature maps for region i from the m-th convolutional branch, where L_m is the uniform output length of the feature maps produced by all filters within that branch. After most convolutional operations (specifically, for local and periodic pattern branches), an adaptive max pooling layer, denoted as $\operatorname{Pool}(\cdot)$, is applied to compress the feature maps along the time axis to a fixed dimension P_u . This helps in controlling the feature size and extracting salient information. Global pattern branches, having already aggregated information across the entire window by design $(L_m = 1)$, are not subjected to further pooling.

All branch outputs are then flattened along their temporal dimension and concatenated. The concatenated feature vector is subsequently passed through a non-linear activation function, $Activation(\cdot)$ (e.g., hyperbolic tangent), to form the final temporal feature embedding for region i:

$$\mathbf{h}_{i}^{temp} = \operatorname{Activation} \left(\operatorname{Concat}_{m=1}^{M} \left[\operatorname{Flatten} (\operatorname{Pool}_{m}(\mathbf{X}_{i}^{(m)})) \right] \right)$$
 (2)

where Pool_m applies pooling if $L_m > 1$. The resulting temporal feature embedding for each region is $\mathbf{h}_i^{temp} \in \mathbb{R}^D$. The total feature dimension D for a single region is the sum of the flattened dimensions from all M branches. That is, $D = \sum_{m=1}^M (k \times P'_m)$, where P'_m is P_u for pooled branches, and 1 for non-pooled branches. The specific number of branches for each category (M_L, M_P, M_G) , their respective kernel sizes (s_l, s_p, s_g) , dilation rates (r_l, r_p, r_g) , filter count k, and pooling dimensions P_u are hyperparameters determined experimentally to best capture the dataset's characteristics, such as periodicity in epidemic data.

• Local Transmission Risk (LTR) Encoding $(A_{i:}^{geo})$

This module quantifies the local transmission risk for each region based on its geographical connectivity. It leverages a geographical adjacency matrix \mathbf{A}^{geo} , where $a^{geo}_{i,j}=1$ signifies that region i and region j are direct neighbors (with $a^{geo}_{i,i}=1$ by default for self-connectivity).

For each region i, its local transmission risk is captured by a vector $\mathbf{h}_i^l \in \mathbb{R}^D$. This encoding is derived from the region's degree, d_i , which is calculated as the sum of elements in the i-th row of the adjacency matrix, $\mathbf{A}_{i:}^{geo}$, i.e., $d_i = \sum_j a_{i,j}^{geo}$. This degree represents the total count of region i's geographical neighbors. The rationale is that a higher degree indicates greater connectivity and centrality, leading to more frequent potential interactions and an elevated likelihood of disease spread.

The local transmission risk encoding is formulated as:

$$\mathbf{h}_i^l = \mathbf{W}^l \cdot d_i + \mathbf{b}^l \tag{3}$$

where $\mathbf{W}^l \in \mathbb{R}^D$ is a learnable weight vector that adjusts the importance of this degree, allowing the model to learn how connectivity translates into a multi-dimensional risk representation. $\mathbf{b}^l \in \mathbb{R}^D$ is a learnable bias vector, also optimized during training, which adjusts the baseline risk for each dimension.

• Global Transmission Risk (GTR) Encoding (H^{temp})

This module evaluates the risk of disease transmission across all regions from a global perspective, capturing potential infection pathways spread beyond local neighbors. These pathways include non-adjacent connections (e.g., regions linked by long-distance travel despite lacking shared borders), cross-regional interactions (e.g., disease spread between distant administrative or geopolitical areas), and periodic patterns (e.g., seasonal fluctuations driven by climate or recurring travel cycles). Following the idea of multiplicative self-attention[18, 19], first, $\mathbf{H}^{temp} = [\mathbf{h}_1^{temp}, \mathbf{h}_2^{temp}, \dots, \mathbf{h}_N^{temp}]^T \in \mathbb{R}^{N \times D}$ is projected into two separate embedding spaces via learned linear transformations $\mathbf{W}^q \in \mathbb{R}^{D \times F}$ and $\mathbf{W}^k \in \mathbb{R}^{D \times F}$ to generate the Query matrix $\mathbf{Q} \in \mathbb{R}^{N \times F}$ and the Key matrix $\mathbf{K} \in \mathbb{R}^{N \times F}$. Here, F denotes the attention projection dimension, representing the size of the latent feature space to which the original input vectors are mapped for computing pairwise attention scores. These matrices allow the model to represent each region in two roles: as a potential receiver (Query) and as a potential transmitter (Key) of infection risk. The Attention Scores matrix $\mathbf{A} \in \mathbb{R}^{N \times N}$ is computed as the dot product between \mathbf{Q} and \mathbf{K}^T , quantifying correlations between all pairs of positions:

$$\mathbf{Q} = \mathbf{H}^{temp} \mathbf{W}^q, \mathbf{K} = \mathbf{H}^{temp} \mathbf{W}^k, \mathbf{A} = \mathbf{Q} \mathbf{K}^{\mathrm{T}}$$
(4)

After being normalized, $a_{i,j}$ represents the transmission risk of region j to region i:

$$a_{i,j} = \frac{a_{i,j}}{\max(||\mathbf{a}_{i:}||_2, \epsilon)} \tag{5}$$

where $\mathbf{a}_{i:} \in \mathbb{R}^N$ is the *i*-th row of matrix \mathbf{A} , $||\cdot||_2$ is the L_2 norm and ϵ is a small value to prevent division by zero, ensuring numerical stability. By summing all incoming risks $a_{i,j}$ from other regions j, g_i quantifies the aggregated transmission risk of all other regions to region i:

$$g_i = \sum_j a_{i,j} \tag{6}$$

The aggregated risk score g_i is then linearly transformed to produce the final global transmission risk vector $\mathbf{h}_i^g \in \mathbb{R}^D$ for region i:

$$\mathbf{h}_i^g = \mathbf{W}^g \cdot g_i + \mathbf{b}^g \tag{7}$$

where $\mathbf{W}^g \in \mathbb{R}^D$ and $\mathbf{b}^g \in \mathbb{R}^D$ are trainable parameters, randomly initialized and optimized during training.

• Region-Aware Graph Learner $(\mathbf{h}_i^{temp}, \mathbf{h}_i^{temp}, \mathbf{A}^{geo}, \mathbf{E})$

First, the model learns an asymmetric temporal correlation graph $\hat{\mathbf{A}}$ from time series data, capturing directed temporal influence between regions. Next, the geographical adjacency matrix \mathbf{A}^{geo} and the region degree information $\mathbf{d} = [d_1, \dots, d_N]^T \in \mathbb{R}^N$ are used as gates to modulate spatial dependencies, resulting in a spatial dependency-aware correlation matrix \mathbf{A}^{spa} . If external resources (e.g., human mobility data or environmental factors) are available, they are encoded as an external correlation matrix \mathbf{A}^e , further enriching the model's understanding of true inter-region interactions. The final propagation graph is constructed by summing $\hat{\mathbf{A}}$, \mathbf{A}^{spa} and \mathbf{A}^e , forming the ultimate propagation graph structure. Using broadcasting, dynamic temporal relationships are extracted by:

$$\mathbf{M}_1 = \tanh(\mathbf{H}^{temp}\mathbf{W}_1 + \mathbf{b}_1), \quad \mathbf{M}_2 = \tanh(\mathbf{H}^{temp}\mathbf{W}_2 + \mathbf{b}_2) \in \mathbb{R}^{N \times F}$$
 (8)

$$\hat{\mathbf{A}} = \text{ReLU}(\text{tanh}(\mathbf{M}_1 \mathbf{M}_2^{\text{T}} - \mathbf{M}_2 \mathbf{M}_1^{\text{T}})) \in \mathbb{R}^{N \times N}$$
(9)

where $\mathbf{W_1}, \mathbf{W_2} \in \mathbb{R}^{D \times F}$ are weight matrices and $\mathbf{b_1}, \mathbf{b_2} \in \mathbb{R}^{1 \times F}$ are bias vectors. Spatial dependency combines the geographical adjacency matrix with degree gating:

$$\mathbf{D}^* = \operatorname{sigmoid}(\mathbf{W}^* \odot \mathbf{dd}^{\mathrm{T}}) \in \mathbb{R}^{N \times N}$$
(10)

$$\mathbf{A}^{spa} = \mathbf{D}^* \odot \mathbf{A}^{geo} \in \mathbb{R}^{N \times N} \tag{11}$$

where \odot denotes element-wise multiplication and $\mathbf{W}^* \in \mathbb{R}^{N \times N}$ is the learnable parameter matrix. After fusing external resources (e.g., human mobility data $\mathbf{E} = [\mathbf{E_1}, \mathbf{E_2}, \dots, \mathbf{E_t}]$, where $\mathbf{E}_z \in \mathbb{R}^{N \times N}$ is the correlation matrix at time step z):

$$\mathbf{A}^e = \mathbf{W}^e \odot \sum_{i=0}^{e-1} \mathbf{E}_{t-i} \in \mathbb{R}^{N \times N}$$
 (12)

$$\tilde{\mathbf{A}} = \hat{\mathbf{A}} + \mathbf{A}^{spa} + \mathbf{A}^e \tag{13}$$

where e is the look-back window of external resources, and $\mathbf{W}^e \in \mathbb{R}^{N \times N}$ is a learnable matrix.

• Graph Convolution Network $(\mathbf{h}_i^{feat}, \tilde{\mathbf{A}})$

The temporal feature \mathbf{h}_{i}^{temp} , local transmission risk encoding \mathbf{h}_{i}^{l} , and global transmission

risk encoding \mathbf{h}_{i}^{g} for region i are summed to obtain \mathbf{h}_{i}^{feat} , which serves as the initial representation for each region node.

$$\mathbf{h}_{i}^{feat} = \mathbf{h}_{i}^{temp} + \mathbf{h}_{i}^{l} + \mathbf{h}_{i}^{g} \in \mathbb{R}^{D}$$
(14)

Using the propagation graph structure $\tilde{\mathbf{A}}$ constructed in the previous stage, the node representation for each layer is updated as follows to obtain the node representation $\mathbf{h}_{i}^{(l)}$ for region i at layer l, providing structured spatio-temporal feature input for the final prediction layer.

$$\mathbf{H}^{(l)} = \sigma(\tilde{\mathbf{D}}^{-1}\tilde{\mathbf{A}}\mathbf{H}^{(l-1)}\mathbf{W}^{(l-1)}) \in \mathbb{R}^{N \times D}$$
(15)

where $\mathbf{H}^{(0)} = \mathbf{H}^{feat} = [\mathbf{h}_1^{feat}, \mathbf{h}_2^{feat}, \dots, \mathbf{h}_N^{feat}]^T \in \mathbb{R}^{N \times D}$, $\mathbf{W}^{(l)} \in \mathbb{R}^{D \times D}$ is the weight matrix, $\tilde{\mathbf{D}} \in \mathbb{R}^{N \times N}$ is the degree matrix of $\tilde{\mathbf{A}}$, and σ is a non-linear activation function (e.g., ELU).

• Output $(\mathbf{x}_{i:}, [\mathbf{h}_i^{feat}; \mathbf{h}_i^{(L)}])$

Finally, the GCN input \mathbf{h}_{i}^{feat} is concatenated with the last layer's output $\mathbf{h}_{i}^{(L)}$ (L denotes the last layer), passed through a fully connected layer to obtain the non-linear prediction result $\hat{y}_{i,t+h}^{nl}$.

$$\hat{\mathbf{y}}_{t+h}^{nl} = [\mathbf{H}^{(0)}; \mathbf{H}^{(L)}] \mathbf{W}^{nl} + \mathbf{b}^{nl} \in \mathbb{R}^{N}$$
(16)

where $[\cdot;\cdot]$ denotes feature concatenation. $\mathbf{W}^{nl} \in \mathbb{R}^{2D}$ and $\mathbf{b}^{nl} \in \mathbb{R}^{N}$ are the parameters. The linear prediction result from the AR module (optional) $\hat{\mathbf{y}}_{t+h}^{ar} \in \mathbb{R}^{N}$ and the non-linear prediction result from the GCN output $\hat{\mathbf{y}}_{t+h}^{nl}$ are summed to obtain the final predicted value $\hat{\mathbf{y}}_{t+h}$.

$$\hat{y}_{i,t+h}^{ar} = \sum_{\beta=0}^{q-1} \mathbf{W}_{\beta}^{ar} \cdot x_{i,t-\beta} + b^{ar}$$
(17)

$$\hat{\mathbf{y}}_{t+h} = \hat{\mathbf{y}}_{t+h}^{ar} + \hat{\mathbf{y}}_{t+h}^{nl} \tag{18}$$

where $\mathbf{W}^{ar} \in \mathbb{R}^q$ and $b^{ar} \in \mathbb{R}$ are the parameters in AR component, and q is the look-back window of AR. The loss function is the mean squared error:

$$Loss(\Theta) = ||\mathbf{y}_{t+h} - \hat{\mathbf{y}}_{t+h}||_2^2 \tag{19}$$

where Θ represents the set of all trainable parameters, \mathbf{y}_{t+h} is the ground truth value, and $||\cdot||_2^2$ is squared L_2 norm.

3.3 ColaGNN Model Framework

ColaGNN is a class of Graph Neural Network models specifically designed for long-term influenza forecasting. Its main features include a temporal dependency modeling, a cross-location attention mechanism and a graph-based feature propagation mechanism, aiming to enhance the ability to model complex long-term trends and dependencies between non-adjacent regions[14]. Its overall structure is as follows:

• Temporal Dependency Modeling Module

This module integrates two complementary approaches to capture diverse temporal information from the historical time series of each region: RNN for long-term sequence aggregation and CNN for multi-scale local pattern extraction.

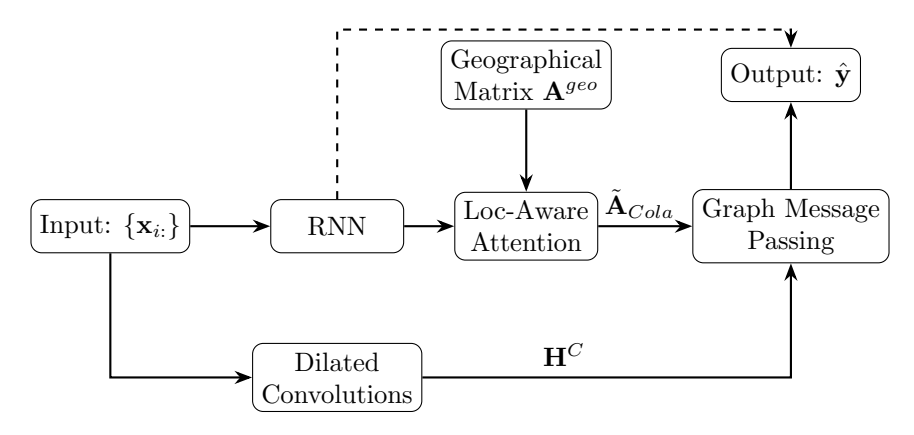


Figure 2: ColaGNN workflow

- Long-term Sequence Aggregation: RNN Module (x_i.)

The purpose of this module is to capture comprehensive long-term dependencies and sequential information from the entire historical time series of each region, treating the data as a continuous sequence. For each region i, its historical input sequence $\mathbf{x}_{i:} = [x_{i,t-T+1},...,x_{i,t}]$ is fed into an RNN model (e.g., GRU [15] or LSTM [16]) with shared parameters across regions. The RNN aggregates and learns all features of historical time steps equally, updating its hidden state $\mathbf{h}_{i,t'}$ at each time step. The final hidden state $\mathbf{h}_{i,t}$ serves as the holistic temporal representation for region i. Let D' be the dimension of the hidden state. The RNN updates the hidden state at time t'.

$$\mathbf{h}_{i,t'} = \tanh(\mathbf{w}x_{i,t'} + \mathbf{U}\mathbf{h}_{i,t'-1} + \mathbf{b}) \in \mathbb{R}^{D'}$$
(20)

where $\mathbf{h}_{i,t'}$ and $\mathbf{h}_{i,t'-1}$ are the hidden states at time t' and t'-1, respectively, tanh is the non-linear activation function, $\mathbf{w} \in \mathbb{R}^{D'}$, $\mathbf{U} \in \mathbb{R}^{D' \times D'}$, $\mathbf{b} \in \mathbb{R}^{D'}$ are trainable weights and biases. The last hidden state $\mathbf{h}_{i,t}$ serves as the representation for location i, used for subsequent attention calculation.

- Local Pattern Extraction: Multi-Scale Convolutional Module (ColaGNN's) This module is designed to extract important local and multi-scale feature patterns from the time series $\mathbf{x}_{i:} \in \mathbb{R}^{1 \times T}$ for region i using two parallel one-dimensional convolutional branches: one for capturing short-term patterns and another for long-term patterns. Each branch employs k' filters. For a filter $\mathbf{c}^{(r',n')} \in \mathbb{R}^{s'}$ (where $n' = 1, \ldots, k'$ is the filter index, s' is the kernel size, and r' is the dilation rate), the convolution operation at step j for location i is:

$$\mathbf{d}_{i}^{(r',n')}[j] = \sum_{p=0}^{s'-1} \mathbf{x}_{i:}[j+r' \times p] \cdot \mathbf{c}^{(r',n')}[p]$$
(21)

Here, $\mathbf{d}_i^{(r',n')}$ represents the output feature vector for the n'_{th} filter with dilation rate r'. The output length of a 1D convolution L_{out} given input length T, kernel size s', and dilation rate r' (with stride 1 and padding 0) is calculated as $L_{out} = T - r' \times (s' - 1)$. The two convolutional branches are configured with distinct kernel sizes and dilation rates:

* Short-term Pattern Branch: This branch is designed to capture immediate, fine-grained temporal dependencies or overall trends spanning the entire input

window. It achieves this by utilizing a relatively large kernel size s'_{short} (e.g., matching the input length T) and a small dilation rate r'_{short} (typically 1). For each of its k' filters, this branch generates an output feature map $\mathbf{d}_i^{(r'_{short}, n')} \in \mathbb{R}^{L_{short}}$, where $L_{short} = T - r'_{short} \times (s'_{short} - 1)$.

* Long-term Pattern Branch: This branch focuses on capturing more distant, sparse, or periodic dependencies over a broader temporal range. It achieves this by employing a relatively smaller kernel size s'_{long} but a larger dilation rate r'_{long} ($r'_{long} > r'_{short}$). The larger dilation rate effectively expands the receptive field without increasing the number of parameters, allowing the filter to skip intermediate time steps and focus on distant patterns. For each of its k' filters, this branch generates an output feature map $\mathbf{d}_i^{(r'_{long},n')} \in \mathbb{R}^{L_{long}}$, where $L_{long} = T - r'_{long} \times (s'_{long} - 1)$.

The outputs from all filters across both branches are flattened and concatenated. This combined feature vector is then passed through a Rectified Linear Unit (ReLU) activation function to form the final temporal feature embedding \mathbf{h}_i^C :

$$\mathbf{h}_{i}^{C} = \text{ReLU}\left\{\text{Concat}\left[\mathbf{d}_{i}^{(r'_{short},1)}, \dots, \mathbf{d}_{i}^{(r'_{short},k')}, \mathbf{d}_{i}^{(r'_{long},1)}, \dots, \mathbf{d}_{i}^{(r'_{long},k')}\right]\right\}$$
(22)

The concatenated outputs form $\mathbf{h}_i^C \in \mathbb{R}^{F^{(0)}}$. The total feature dimension $F^{(0)}$ for a single region i after these multi-scale convolutions and concatenation is calculated as:

$$F^{(0)} = k' \times (L_{short} + L_{long}) \tag{23}$$

The specific kernel sizes (s'_{short}, s'_{long}) , dilation rates (r'_{short}, r'_{long}) , and number of filters k' are hyperparameters determined experimentally to best capture the dataset's characteristics, such as periodicity in epidemic data.

- Cross-Regional Influence Modeling Module: Loc-Aware Attention $(h_{i,t}, h_{j,t}, \mathbf{A}^{geo})$ The purpose of this module is to capture dynamic propagation relationships between regions, not limited to fixed geographical adjacency. For each pair of regions (i, j), an asymmetric attention weight $a'_{i,j}$ is calculated based on their historical hidden states $h_{i,t}$ and $h_{j,t}$, combined with the geographical adjacency matrix \mathbf{A}^{geo} , forming a location-aware dynamic adjacency matrix. This module introduces a gating mechanism to fuse static geographical adjacency with dynamic propagation trends.
 - General Attention Calculation Mechanism:

Based on RNN hidden states, additive attention [17] is used to calculate the influence of location j on location i:

$$a'_{i,j} = \mathbf{v}^{\mathrm{T}} \Delta (\mathbf{W}' \mathbf{h}_{i,t} + \mathbf{W}'' \mathbf{h}_{j,t} + \mathbf{b}') + b^{v}$$
(24)

where Δ is an element-wise activation function (e.g., ELU), $\mathbf{W}', \mathbf{W}'' \in \mathbb{R}^{d_a \times D'}$ are weight matrices, d_a is a hyperparameter, $\mathbf{v} \in \mathbb{R}^{d_a}, \mathbf{b}' \in \mathbb{R}^{d_a}, b^v \in \mathbb{R}$ are trainable parameters, and $a'_{i,j}$ is the attention coefficient, representing the influence of j on i. The resulting asymmetric attention matrix $\mathbf{A}' \in \mathbb{R}^{N \times N}$ has each row representing the influence of other locations on the current location. To normalize the overall influence of different locations, $L_{p'}$ norm normalization is applied row-wise:

$$\mathbf{a}_{i:}' \leftarrow \frac{\mathbf{a}_{i:}'}{\max(||\mathbf{a}_{i:}'||_{p'}, \epsilon)} \tag{25}$$

where $||\cdot||_{p'}$ is the $L_{p'}$ norm (in experiments, p'=2).

- Location-Aware Fusion Mechanism (Gate):

To enhance geographical interpretability, the static geographical adjacency matrix \mathbf{A}^{geo} is introduced and normalized, allowing the model to consider both data-driven correlations and existing geographical information without excessive deviation. The attention results are weighted and fused with the original geographical adjacency matrix to generate a location-aware attention matrix $\tilde{\mathbf{A}}_{Cola}$, preserving both historical dynamics and geographical priors.

$$\tilde{\mathbf{A}}^{geo} = \mathbf{D}^{-\frac{1}{2}} \mathbf{A}^{geo} \mathbf{D}^{-\frac{1}{2}} \in \mathbb{R}^{N \times N}$$
 (26)

where $\mathbf{D} \in \mathbb{R}^{N \times N}$ is the degree matrix of \mathbf{A}^{geo} defined as $d_{ii} = \sum_{j=1}^{N} a_{ij}^{geo}$. The gating matrix \mathbf{M} is learned based on the general attention matrix \mathbf{A}' :

$$\mathbf{M} = \operatorname{Sigmoid}(\mathbf{W}^M \mathbf{A}' + b^M \mathbf{1}_N \mathbf{1}_N^{\mathrm{T}})$$
 (27)

where $\mathbf{W}^M \in \mathbb{R}^{N \times N}, b^M \in \mathbb{R}$ are trainable parameters, and $\mathbf{1}_N \in \mathbb{R}^N$ is an N-dimensional vector whose elements are all 1_s . The final location-aware attention matrix is:

$$\tilde{\mathbf{A}}_{Cola} = \mathbf{M} \odot \tilde{\mathbf{A}}^{geo} + (\mathbf{1}_N \mathbf{1}_N^{\mathrm{T}} - \mathbf{M}) \odot \mathbf{A}' \in \mathbb{R}^{N \times N}$$
(28)

 $\tilde{\mathbf{A}}_{Cola}$ dynamically balances geographical adjacency and historical data-driven attention, enhancing the model's ability to capture non-adjacent regional dependencies.

• Graph Message Passing $(\mathbf{h}_i^C, \tilde{\mathbf{A}}_{Cola})$

The purpose of this module is to integrate neighborhood information and model potential correlated propagation patterns between regions. The location-aware adjacency matrix $\tilde{\mathbf{A}}_{Cola}$ generated in the previous step serves as the graph structure, and temporal features are used as node features for graph neural network propagation. Dilated convolutional features \mathbf{h}_i^C act as initial node features $\hat{\mathbf{h}}_i^{(0)}$, performing graph message passing where each node receives (weighted) information updates from neighbors to obtain a comprehensive representation that incorporates the influence of surrounding regions:

$$\hat{\mathbf{h}}_{i}^{(l)} = \text{ReLU}\left(\sum_{j \in \mathcal{N}} a_{i,j}^{"} \hat{\mathbf{W}}^{(l-1)} \hat{\mathbf{h}}_{j}^{(l-1)} + \mathbf{b}^{(l-1)}\right)$$
(29)

where $\hat{\mathbf{h}}_{j}^{(l-1)} \in \mathbb{R}^{F^{(l-1)}}$ is node feature of node j at layer l-1, $a_{i,j}''$ is the (i,j) element of $\tilde{\mathbf{A}}_{Cola}$, $\hat{\mathbf{W}}^{(l-1)} \in \mathbb{R}^{F^{(l)} \times F^{(l-1)}}$ is the weight matrix for hidden layer l with $F^{(l)}$ feature maps, $\mathbf{b}^{(l-1)} \in \mathbb{R}^{F^{(l)}}$ is the bias, and \mathscr{N} is the set of locations. Multi-layer message passing (2 layers in experiments) updates node representations, capturing inter-regional propagation dynamics.

• Output $([\mathbf{h}_{i,t}; \hat{\mathbf{h}}_i^{(L')}])$

The result after graph propagation $\hat{\mathbf{h}}_i^{(L')}$ (L' denotes the last layer) is concatenated with the RNN hidden state $\mathbf{h}_{i,t}$ and used as the final input. A linear layer outputs the prediction of future values:

$$\hat{y}_i = \mathbf{W}_o^T [\mathbf{h}_{i,t}; \hat{\mathbf{h}}_i^{(L')}] + b_o \tag{30}$$

where $\mathbf{W}_o \in \mathbb{R}^{D'+F^{(L')}}, b_o \in \mathbb{R}$ are trainable parameters.

• Loss Function

To prevent overfitting in small-sample scenarios, ColaGNN additionally incorporates an L2 regularization term into the loss function, which penalizes large model parameters, ensuring sparsity and robustness. The complete loss function is as follows:

$$Loss(\Theta') = \sum_{i=1}^{N} \sum_{m_i=1}^{n_i} |y_{i,m_i} - \hat{y}_{i,m_i}| + \lambda \Re(\Theta')$$
(31)

where n_i is the number of samples in location i obtained by a moving window, shared by all locations, y_{i,m_i} is the true value of location i in sample m_i , and \hat{y}_{i,m_i} is the model prediction. $\Re(\Theta')$ is the regularization term, and Θ' represents the set of all trainable parameters in the model. The impact of the regularization term on the total loss can be adjusted by controlling the magnitude of the regularization coefficient λ .

4 Experiments and Analysis

Below, we will conduct experiments on EpiGNN and ColaGNN models using four different datasets and compare their prediction performance under various metrics.

4.1 Experimental Setup

- Datasets: Three influenza datasets (Japan-Prefectures, US-Regions, US-States) and one COVID-19 dataset (Australia-COVID). Data is chronologically divided into training (50%), validation (20%), and testing (30%) sets.
 - Australia-COVID: This dataset is obtained from the publicly available JHU-CSSE dataset [20], this dataset records daily new COVID-19 confirmed cases in Australia, encompassing 6 states and 2 territories, from January 27, 2020, to August 4, 2021.
 - Japan-Prefectures: This dataset is sourced from the Infectious Diseases Weekly Report (IDWR) in Japan [21], providing weekly influenza-like-illness (ILI) statistics (patient counts) across 47 prefectures from August 2012 to March 2019.
 - US-Regions: This dataset is derived from the ILINet section of the US-HHS dataset [22], including weekly influenza activity levels for 10 Health and Human Services (HHS) regions across the U.S. mainland, covering the period from 2002 to 2017. Each region aggregates flu patient counts, calculated by combining state-specific data.
 - US-States: This dataset is collected from the Center for Disease Control (CDC) [23], containing weekly counts of patient visits for ILI (positive cases) for each state in the United States from 2010 to 2017. After excluding Florida due to missing data, the dataset retains 49 states.

Datasets	Regions	Length	Min	Max	Mean	SD	Gran.
Japan-Prefectures	47	348	0	26635	655	1711	weekly
US-Regions	10	785	0	16526	1009	1351	weekly
US-States	49	360	0	9716	223	428	weekly
Australia-COVID	8	556	0	9987	539	1532	daily

Table 1: Dataset characteristics summary

• Baseline: STGCN

• Evaluation Metrics: The models use RMSE, MAE, and PCC as evaluation metrics.

$$RMSE = \sqrt{\frac{1}{n} \sum_{i=1}^{n} (\hat{y}_i - y_i)^2}$$

$$MAE = \frac{1}{n} \sum_{i=1}^{n} |\hat{y}_i - y_i|$$

$$PCC = \frac{\sum_{i=1}^{n} (\hat{y}_i - \overline{\hat{y}})(y_i - \overline{y})}{\sqrt{\sum_{i=1}^{n} (\hat{y}_i - \overline{\hat{y}})^2} \sqrt{\sum_{i=1}^{n} (y_i - \overline{y})^2}}$$

- Hyperparameters: Look-back window T = 20, prediction horizons $h = \{2, 5, 8, 11, 14, 17, 20, 23, 26, 29, 32\}$, batch size 128. To improve training stability and convergence speed, the Adam optimizer [24] (Adaptive Moment Estimation) is introduced to dynamically adjust the learning rate: initial learning rate 0.001, weight decay 5e 4. To further enhance the model's generalization ability, Dropout and Early Stopping are incorporated during training: Dropout = 0.2, Early Stopping = 100.
- Environment: Our experiments were conducted on a Windows server equipped with an Nvidia 2060 GPU, leveraging CUDA 11.8 for GPU acceleration. The core computational framework utilized was PyTorch 2.2.1. The following key Python packages were instrumental in our implementation and analysis:
 - pandas (version 2.2.3): Employed for efficient data manipulation and analysis.
 - numpy (version 1.26.4): Used for fundamental numerical operations and array processing.
 - scikit-learn (version 1.4.2): Utilized for various machine learning utilities, including model evaluation metrics.
 - scipy (version 1.15.2): Provided advanced scientific computing functionalities, such as sparse matrix operations and statistical tools.
 - tensorboardX (version 2.6.2.2): Integrated for experiment tracking, visualization of training progress, and logging.
 - torch_geometric (version 2.6.1): Specifically used for implementing graph neural network components and handling graph data structures.

4.2 Prediction Performance

• Australia-COVID Dataset Prediction Analysis (daily)



Figure 3: Prediction performance on Australia-COVID dataset

Method	Metric						horizon					
		2	5	8	11	14	17	20	23	26	29	32
EpiGNN	MAE RMSE PCC	127.2462 388.4988 0.9942	124.475 341.19 0.9925	$100.546 \\ 315.349 \\ 0.9919$	$112.6527 \\ 370.0045 \\ 0.9905$	163.1471 495.6291 0.9887	170.5775 513.5239 0.9864	194.5076 573.451 0.9863	212.0276 617.045 0.984	210.8035 614.6236 0.981	281.8333 725.7447 0.9816	304.4768 828.0177 0.9834
ColaGNN	MAE RMSE PCC	38.5352 180.3111 0.9974	$68.965 \\ 276.612 \\ 0.9948$	117.77 434.282 0.9882	129.8169 458.9208 0.9878	149.3325 523.0732 0.9828	154.6378 546.5959 0.9798	116.4481 450.783 0.9833	142.1623 513.2499 0.9798	145.512 547.5059 0.9747	129.1289 499.4233 0.9781	$108.8203 \\ 430.2485 \\ 0.9841$
STGCN	MAE RMSE PCC	451.3148 1052.659 0.8412	229.833 601.93 0.9829	295.414 796.312 0.9622	335.3027 911.3586 0.9763	305.1303 842.0427 0.9835	268.4486 723.162 0.985	679.8415 1837.4347 0.8897	190.1576 572.1667 0.9833	245.7612 716.6028 0.9818	268.5856 683.0385 0.9743	413.9621 919.0851 0.8863

Table 2: Performance Comparison of Epidemic Prediction Models in Australia. Bold face indicates the best result of each column.

The analysis of the Australia-COVID dataset reveals distinct strengths and weaknesses across the EpiGNN, ColaGNN, and STGCN models, as detailed in Table 2 and further illustrated in Figure 3. EpiGNN shows its strength in the short-to-mid-term (Horizon 8–17), achieving its lowest error at Horizon 8 and demonstrating a highly consistent PCC that indicates stable trend-fitting. Conversely, ColaGNN is superior for long-term (Horizon ¿ 20) predictions, where it maintains significantly lower errors. Although EpiGNN is strong in a specific mid-range, its errors escalate substantially in later horizons, highlighting ColaGNN's more robust predictive stability across the full forecast window. In contrast, STGCN exhibited drastic fluctuations across all metrics, with large and unstable errors and poor trend correlation, lacking reliable predictive performance.

• Japan Dataset Prediction Analysis (weekly)

Method	Metric						horizon					
		2	5	8	11	14	17	20	23	26	29	32
EpiGNN	MAE	317.7547	421.4113	534.7141	667.254	532.3716	600.1184	740.9535	589.0948	527.1279	572.4716	566.4541
	RMSE	934.0154	1051.202	1259.9516	1639.9694	1464.4508	1660.7635	1678.3348	1403.6164	1455.9536	1551.2411	1454.3491
	PCC	0.9168	0.9016	0.8531	0.6671	0.7321	0.6517	0.5853	0.7966	0.792	0.722	0.7077
ColaGNN	MAE	287.5924	379.4594	412.5771	500.2072	491.446	548.1924	519.0634	499.7023	462.7714	492.9672	616.65
	RMSE	948.7436	1152.2875	1275.8528	1421.0287	1412.8741	1484.6521	1471.9136	1388.5836	1361.7301	1540.4139	1657.0711
	PCC	0.9253	0.8628	0.8681	0.7744	0.7812	0.7339	0.8148	0.8098	0.8673	0.6967	0.595
STGCN	MAE	304.3613	433.1643	449.0197	512.6342	538.246	534.1789	521.1423	568.3075	410.4855	518.1366	522.0048
	RMSE	967.6338	1301.5097	1353.251	1492.7615	1598.077	1651.6565	1565.2718	1434.4414	1275.8279	1455.7326	1498.1865
	PCC	0.9071	0.8382	0.8306	0.7687	0.7752	0.7601	0.8233	0.7725	0.8558	0.832	0.757

Table 3: Performance Comparison of Epidemic Prediction Models in Japan

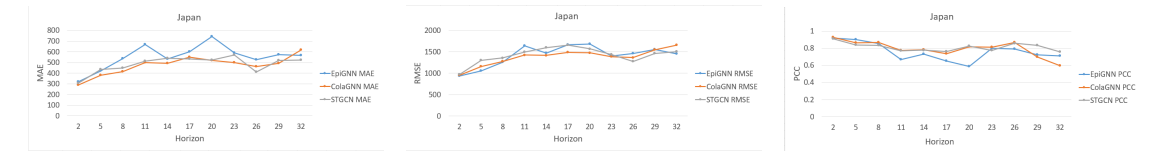


Figure 4: Prediction performance on Japan dataset

The analysis of the Japan-Prefectures dataset is detailed in Table 3 and further illustrated in Figure 4. EpiGNN demonstrates a clear advantage in short-term forecasting (horizons 2, 5, 8), leading in RMSE with values like 934.0154 (horizon 2) and 1051.202 (horizon 5), indicating its ability to minimize large errors in near-term predictions, making it suitable for scenarios requiring precise short-term epidemic trends. ColaGNN consistently demonstrates a strong advantage in MAE across most horizons (especially short to mid-term)

and often excels in RMSE and PCC in the mid-term range, showcasing its superior accuracy and correlation for extended horizons. STGCN, while remains competitive and even achieves the lowest RMSE of all models at horizon 26 and 29, is still not as competitive as ColaGNN.

• US-Regions Dataset Prediction Analysis (weekly)

Method	Metric	ric horizon										
monod	11101110	2	5	8	11	14	17	20	23	26	29	32
EpiGNN	MAE RMSE PCC	271.9734 495.2303 0.9421	543.7277 898.0375 0.7813	$608.6584 \\ 1024.3151 \\ 0.7064$	$693.9379 \\ 1139.753 \\ 0.6038$	$584.1873 \\994.9219 \\0.7312$	$595.4306 \\990.6613 \\0.7339$	812.4983 1278.9443 0.5564	$743.6681 \\1203.0116 \\0.5585$	815.2423 1292.1929 0.5114	679.3557 1043.0071 0.6884	689.5122 989.5857 0.7704
ColaGNN	MAE RMSE PCC	233.6242 506.9187 0.9435	525.8035 1007.5835 0.7988	$685.4155 \\1270.2356 \\0.6637$	786.2728 1407.126 0.6036	$708.7531 \\ 1260.4982 \\ 0.6874$	848.0165 1429.4681 0.46159	878.642 1483.2721 0.4159	$658.7186 \\1061.4983 \\0.6701$	$633.9754 \\1206.7821 \\0.7355$	$484.4075 \\969.8692 \\0.774$	$447.5002 \\904.5961 \\0.7968$
STGCN	MAE RMSE PCC	408.5528 697.2763 0.8783	556.1506 1066.6802 0.7682	701.1787 1267.289 0.6872	784.0956 1384.2491 0.5907	800.3231 1381.3204 0.4352	790.7985 1413.0061 0.6718	$684.8737 \\1235.4878 \\0.7169$	768.8422 1305.1195 0.5499	684.4204 1242.937 0.7164	587.5015 1077.7383 0.7574	523.9285 996.238 0.7571

Table 4: Performance Comparison of Epidemic Prediction Models in US-Regions



Figure 5: Prediction performance on US-Regions dataset

The analysis of the US-Regions dataset is detailed in Table 4 and further illustrated in Figure 5. EpiGNN demonstrates a notable advantage in the short-term prediction phase (Horizon \leq 17). In this range, its RMSE is consistently lower than the other models, such as 990.6613 at horizon 17 compared to ColaGNN's 1429.4681, indicating stronger predictive accuracy. However, as the time horizon extends, ColaGNN establishes clear superiority in the medium to long-term (Horizon \wr 20). In this later phase, its MAE and RMSE are significantly lower and more stable than EpiGNN's and STGCN's. For instance, at horizon 32, ColaGNN's RMSE is 904.5961, while EpiGNN's is 989.5857. Furthermore, its PCC shows a steady improvement in the long term, suggesting better trend consistency. In contrast, STGCN remains volatile across all metrics, exhibiting high errors and multiple correlation troughs, which indicates weak and unreliable predictive performance on this dataset.

• US-States Dataset Prediction Analysis (weekly)

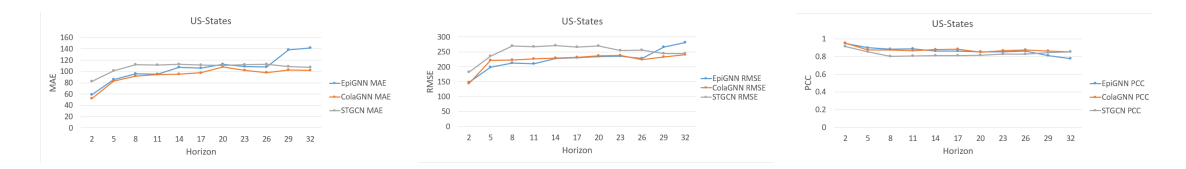


Figure 6: Prediction performance on US-States dataset

The analysis of the US-States dataset is detailed in Table 5 and further illustrated in Figure 6. ColaGNN and EpiGNN exhibit highly competitive performance, especially in

Method	Metric	horizon										
mounoa	11100110	2	5	8	11	14	17	20	23	26	29	32
EpiGNN	MAE	58.6324	85.646	95.9525	94.9318	107.6102	105.6782	112.834	108.9413	107.7824	138.4842	141.8843
	RMSE	148.2381	199.371	212.59	210.8205	228.3557	231.091	234.3161	236.3079	227.6159	265.86	281.6397
	PCC	0.9449	0.8975	0.8827	0.8868	0.8601	0.8602	0.8515	0.8508	0.8607	0.8088	0.7776
ColaGNN	MAE	53.4726	83.3606	91.9288	94.4864	95.2117	97.5189	108.0375	101.7764	97.9957	102.4193	101.776
	RMSE	148.1823	221.7605	223.09	227.3539	229.4957	232.3823	236.4327	238.5425	224.7046	233.7741	241.2217
	PCC	0.9498	0.8747	0.8723	0.8671	0.8797	0.8816	0.849	0.8663	0.8744	0.8613	0.8545
STGCN	MAE	82.7078	101.3556	111.7042	113.3681	112.4669	111.6197	110.8818	11.9671	112.5974	108.3811	107.0486
	RMSE	181.8974	235.4713	270.4545	267.4492	271.1715	266.1554	269.5841	254.2331	255.5211	244.7531	245.1524
	PCC	0.914	0.8517	0.8036	0.807	0.8092	0.8115	0.8138	0.8281	0.8255	0.8453	0.8513

Table 5: Performance Comparison of Epidemic Prediction Models Across in US-States

the short term. ColaGNN consistently achieves the lowest MAE across nearly all stages and demonstrates superior performance in the long term (Horizon \geq 26), where its RMSE remains lower and more stable, and its PCC is consistently higher. This makes it well-suited for stable short-to-long term trend modeling. EpiGNN is very competitive, even outperforming ColaGNN in RMSE during the short-term phase (Horizon 5-11), but its error increases more significantly in the long term (Horizon \geq 29), making it most suitable for short-term, high-precision scenarios. In contrast, STGCN's performance is consistently weaker, with the highest errors and lowest correlation across most of the prediction horizon, indicating insufficient overall predictive stability for this dataset.

Summary: Overall, EpiGNN and ColaGNN each have their strengths, while STGCN performed poorly in this evaluation:

- EpiGNN: Excels in short-term forecasting, showing high accuracy in specific forecast windows on the Australia-COVID, Japan-Prefectures, US-Regions and US-States datasets. Its primary strength lies in high-precision, short-range predictions. However, its performance tends to degrade as the forecast horizon extends, with increasing errors in the long term across most datasets.
- ColaGNN: Demonstrates stronger and more consistent overall performance, establishing itself as the more robust model, particularly for medium to long-term predictions. It achieved the most stable and accurate results in the later stages across all datasets. This makes ColaGNN the preferable choice for tasks requiring stable medium-to-long-term forecasting and reliable overall trend modeling.
- STGCN: Exhibited drastic fluctuations, large errors, and instability in most tests, with poor trend correlation, lacking reliable predictive performance.

Therefore, EpiGNN is preferred for short-term high-precision and handling complex propagation patterns, while ColaGNN performs better in long-term stable forecasting and overall trend modeling.

5 Advantages and Disadvantages Comparison

5.1 Advantages and Disadvantages of EpiGNN

Advantages:

• Strong spatio-temporal modeling capability: Effectively captures temporal and spatial dependencies through multi-scale convolutions and GCNs. The RAGL module further

integrates geographical information and propagation risk, generating an asymmetric correlation graph that avoids the over-smoothing problem of traditional attention mechanisms, performing exceptionally well in complex propagation paths.

- Combination of linear and non-linear components: By combining AR components and GCN outputs, it balances linear patterns (e.g., government intervention effects in COVID-19) and non-linear patterns (e.g., seasonal fluctuations in influenza), enhancing the model's robustness.
- Flexible external resource integration: The model supports integrating external data such as human mobility, improving the accuracy of inter-regional correlations.
- Interpretability and risk identification: LTR and GTR modules provide interpretability of regional propagation risks through quantified indicators, aiding in identifying highrisk areas.

Disadvantages:

- Decreased long-term prediction performance: Experiments show that as the prediction horizon h increases, prediction accuracy decreases, indicating an imbalance in multisource dynamic inputs over long sequences and limited ability to capture long-term propagation dynamics.
- Complex parameter tuning: Multi-scale convolutions, GCN layer counts, and RAGL hyperparameters require careful tuning, increasing model deployment complexity.
- Lack of temporal decay effect: The model does not account for the characteristic that propagation influence decays over time, which may affect the accuracy of long-term predictions.

5.2 Advantages and Disadvantages of ColaGNN

Advantages:

- Long-term forecasting capability: Relies on RNN recursive modeling and a location-aware attention matrix, suitable for medium to long-term trend modeling.
- Dynamic graph structure: The cross-location attention mechanism can dynamically capture complex dependencies between non-adjacent regions.
- Strong interpretability: The attention matrix helps epidemiologists understand disease diffusion patterns.
- **High computational efficiency:** Small number of parameters and fast training speed, suitable for forecasting tasks involving large-scale regions.

Disadvantages:

- Computational overhead of attention mechanism: Although the overall number of parameters is relatively small, the N^2 -level computational overhead of the attention mechanism can still be a challenge when processing a large number of regions.
- Risk of overfitting: The attention mechanism relies on the direct computation of the last hidden state of the RNN. In data-sparse or small-sample scenarios (e.g., some regions in US-Regions), the model may overfit local patterns.

• Lack of explicit risk encoding: Unlike EpiGNN, it does not explicitly encode local and global transmission risks; this information may need to be implicitly learned from spatio-temporal sequences.

5.3 Model Comparison

Overall Comparison: Both EpiGNN and ColaGNN employ multi-scale convolutions to capture temporal patterns and leverage GNN structures to handle spatial dependencies. Both emphasize the importance of dynamic graph structures and attention mechanisms in capturing complex propagation patterns. EpiGNN's highlight lies in its transmission risk encoding module and Region-Aware Graph Learner (RAGL), which allows it to more finely integrate local and global propagation risks and geographical information, performing exceptionally well in epidemics like COVID-19 that are significantly influenced by government interventions. Additionally, EpiGNN's design combining linear AR components enhances its robustness. ColaGNN, on the other hand, focuses more on long-term forecasting, and its cross-location attention mechanism can dynamically capture complex dependencies between non-adjacent regions, which is crucial for predicting long-term disease propagation patterns. ColaGNN also performs well in terms of data efficiency and model complexity. Nevertheless, both models have their limitations. EpiGNN is limited in long-term forecasting, and its hyperparameter tuning is complex. ColaGNN, while excellent in long-term forecasting, does not offer advantages in short-term predictions and lacks more direct risk encoding to guide epidemiological research.

6 Improvement Space and A HybridGNN Model

6.1 Improvement Space

EpiGNN and ColaGNN have significant complementarity in their design philosophies and application focuses:

- Short-term and long-term prediction complementarity: EpiGNN excels in short-term forecasting and handling sudden outbreaks, and its ability to integrate external events allows it to better adapt to rapid changes in the early stages of an epidemic. ColaGNN, on the other hand, focuses on long-term forecasting, and its dilated convolutions and dynamic attention mechanism are more suitable for capturing periodic, seasonal, and other long-term patterns.
- Explicit risk encoding versus dynamic attention: EpiGNN explicitly designs a transmission risk encoding module, incorporating local and global propagation risks into the model, which provides a more direct perspective for understanding the "causes" and "effects" of disease propagation. While ColaGNN's dynamic attention mechanism can also capture this information, it learns implicitly, making it slightly less interpretable. Combining the two can achieve more comprehensive risk awareness.
- External data integration complementarity: EpiGNN explicitly supports the integration of external data, which is highly beneficial for scenarios with abundant external data. ColaGNN currently primarily relies on existing data, but its dynamic graph learning framework can, in principle, also integrate similar information. Combining EpiGNN's external data integration capabilities with ColaGNN's efficient dynamic graph learning can build a more powerful model.

Based on the strong complementarity between the two in these three aspects, a new model structure can be designed to integrate their respective advantages and compensate for their shortcomings, thereby achieving more effective epidemic forecasting. The EpiCola-GNN model integrates EpiGNN's strengths in risk encoding and local-aware convolutions with ColaGNN's characteristics in long-term forecasting and dynamic attention mechanisms, forming a unified, adaptive spatio-temporal data prediction model designed to handle complex spatio-temporal propagation problems.

6.2 EpiCola-GNN Structure Overview

The core design idea of EpiCola-GNN is:

- Multi-scale temporal feature extraction: Utilizes ColaGNN's multi-scale dilated convolutions, which include short-term and long-term receptive fields, to comprehensively capture temporal features from raw time series data, crucial for disease propagation and other long-term prediction tasks.
- Transmission risk encoding: Borrows from EpiGNN's Global Transmission Risk (GTR) and Local Transmission Risk (LTR) modules, quantifying and encoding potential propagation risks between regions through attention mechanisms and geographical degree information.
- Dynamic graph construction: Combines ColaGNN's RNN-based temporal hidden stategenerated location-aware attention mechanism with normalized geographical adjacency matrices and EpiGNN's degree gating mechanism to dynamically construct and adaptively adjust inter-regional connection strengths, forming the final graph structure.
- Feature fusion and graph message passing: Concatenates multi-scale temporal features, LTR, and GTR encodings to form initial node features for each region. These features are then propagated and learned through multiple layers of Graph Convolutional Networks (GCNs) on the dynamically constructed graph structure.
- Multi-layer GCN propagation: Employs a multi-layer GCN architecture, enabling node features to effectively aggregate neighbor information and transform node features under the guidance of the dynamic Laplacian matrix. The model supports residual connections to preserve information learned at each layer.
- Integrated prediction: In the final prediction stage, the spatio-temporal features processed by GCN are fused with the pure temporal hidden states extracted by RNN. Additionally, the model can optionally include residual connections based on historical raw input data to enhance prediction accuracy and stability.

6.3 EpiCola-GNN Module Details

The specific modules of the model and their operations are shown in Figure 7:

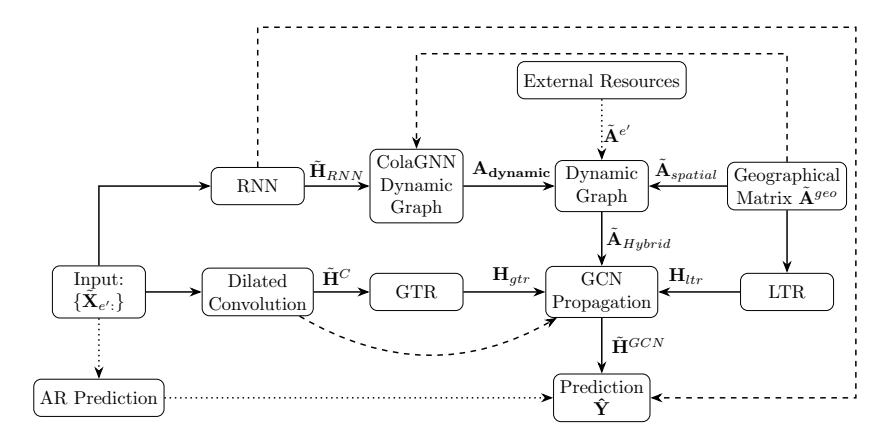


Figure 7: EpiCola-GNN workflow

• Convolutional Temporal Feature Extraction (based on Cola-GNN)

This module extracts short-term and long-term temporal patterns from the time series $\hat{\mathbf{X}} \in \mathbb{R}^{B \times T \times N}$ for N regions, batch size B, and time window T, using one-dimensional dilated convolutions. For each region $e' = 1, \ldots, N$, the time series $\hat{\mathbf{X}}_{e'} \in \mathbb{R}^{B \times T \times 1}$ is reshaped to $\tilde{\mathbf{X}}_{e'} \in \mathbb{R}^{B \times 1 \times T}$ for convolution:

$$\tilde{\mathbf{h}}_{e'}^{C} = \text{Flatten}(\text{Concat}(\text{Conv1d}_{short}(\tilde{\mathbf{X}}_{e':}), \text{Conv1d}_{long}(\tilde{\mathbf{X}}_{e':})))$$
(32)

Here, Conv1d_{short} uses k'' filters with kernel size T and dilation r''=1, producing an output of shape $\mathbb{R}^{B\times k''\times 1}$. Conv1d_{long} uses k'' filters with kernel size $\lfloor T/2 \rfloor$ and dilation r''=2, producing an output of shape $\mathbb{R}^{B\times k''\times (T-2(\lfloor T/2\rfloor-1))}$. Concatenation and flattening yield $\hat{\mathbf{h}}_{e'}^C\in\mathbb{R}^{B\times (k''\cdot (1+(T-2(\lfloor T/2\rfloor-1))))}$. Then, the temporal features of all regions are stacked along the region dimension:

$$\tilde{\mathbf{H}}^C = \text{ReLU}(\text{Stack}([\tilde{\mathbf{h}}_1^C, \dots, \tilde{\mathbf{h}}_N^C])) \in \mathbb{R}^{B \times N \times D_c}$$
(33)

where $D_c = k''(1 + (T - 2(|T/2| - 1))).$

• Dynamic Temporal Feature Extraction (RNN)

For dynamic temporal features, $\hat{\mathbf{X}}$ is reshaped to $\mathbf{X}_{\text{reshape}} \in \mathbb{R}^{(B \cdot N) \times T \times 1}$ and fed to a RNN (LSTM, GRU, or RNN):

$$\tilde{\mathbf{H}}_{RNN} = \text{Reshape}\left(\text{RNN}(\mathbf{X}_{\text{reshape}})[:, -1, :]\right)$$
 (34)

The RNN, with hidden size n_{hidden} , and bidirectional flag bi, outputs $\mathbb{R}^{(B \cdot N) \times T \times D_h}$, where $D_h = n_{hidden} \cdot (1 + bi)$. The last hidden state is abstracted by [:, -1, :] and then reshaped to $\tilde{\mathbf{H}}_{\text{RNN}} \in \mathbb{R}^{B \times N \times D_h}$, used for dynamic graph construction and final prediction.

• Transmission Risk Encoding (based on EpiGNN)

Given the region-wise degree vector $\mathbf{d} \in \mathbb{R}^N$ derived from the geographical adjacency matrix \mathbf{A}^{geo} , and the temporal features $\tilde{\mathbf{H}}^C$, we calculate both the local transmission risk \mathbf{H}_{ltr} and global transmission risk \mathbf{H}_{qtr} .

$$\mathbf{H}_{ltr} = \text{Linear}(\text{Expand}(\mathbf{d})) \in \mathbb{R}^{B \times N \times hidR}$$
 (35)

where hidR is the feature embedding dimension for transmission risk encoding. Expand(\mathbf{d}) $\in \mathbb{R}^{B \times N \times 1}$ broadcasts \mathbf{d} across batch size B to make it suitable for batch processing and

Linear(·) is a linear transformation mapping $\mathbb{R}^1 \to \mathbb{R}^{hidR}$, yielding $\mathbf{H}_{ltr} \in \mathbb{R}^{B \times N \times hidR}$.

$$\mathbf{Attn}_{\mathbf{gtr}} = \text{Normalize}((\tilde{\mathbf{H}}^C \mathbf{W}_{\mathbf{Q}})(\tilde{\mathbf{H}}^C \mathbf{W}_{\mathbf{K}})^T, \text{dim}=-1)$$
(36)

$$\mathbf{H}_{atr} = \operatorname{Linear}(\operatorname{Sum}(\mathbf{Attn_{gtr}}, \operatorname{dim}=-1)) \in \mathbb{R}^{B \times N \times hidR}.$$
 (37)

For global risk, $\mathbf{W}_{\mathbf{Q}}$, $\mathbf{W}_{\mathbf{K}} \in \mathbb{R}^{D_c \times hidA}$ are weight matrices projecting $\tilde{\mathbf{H}}^C$ to $\mathbb{R}^{B \times N \times hidA}$, producing query and key matrices. hidA is the attention hidden dimension for global transmission risk. Their batch matrix product yields $\mathbf{Attn}_{\mathbf{gtr}} \in \mathbb{R}^{B \times N \times N}$. Normalize(\cdot , dim=-1) performs L_2 normalization along the last dimension. Sum(\cdot ,dim=-1) summing along the last dimension gives $\mathbb{R}^{B \times N \times 1}$, which Linear(\cdot) maps to $\mathbf{H}_{atr} \in \mathbb{R}^{B \times N \times hidR}$.

• Dynamic Graph Construction (fusion of EpiGNN and ColaGNN)

This module uses ColaGNN's RNN and additive attention mechanisms fused with EpiGNN geographical adjacency and the external relation matrix to generate a dynamic adjacency matrix for GNN propagation, combining temporal dynamics and geographical priors.

- ColaGNN-style Dynamic Graph (A_{dynamic}):

Using $\tilde{\mathbf{H}}_{RNN} \in \mathbb{R}^{B \times N \times D_h}$ from the temporal module, the additive attention is:

$$\mathbf{A}_{ij}^{P} = \text{Normalize}(\text{ELU}((\tilde{\mathbf{H}}_{RNN})_{i}\mathbf{W}_{\mathbf{p_{1}}}^{\mathbf{T}} + (\tilde{\mathbf{H}}_{RNN})_{j}\mathbf{W}_{\mathbf{p_{2}}}^{\mathbf{T}} + \mathbf{b}_{\mathbf{p_{1}}})\mathbf{V}_{\mathbf{p}} + b_{pv}) \in \mathbb{R}^{B \times 1}$$
(38)

Here, $(\tilde{\mathbf{H}}_{RNN})_i \in \mathbb{R}^{B \times 1 \times D_h}$ is the hidden state for location i. $\mathbf{W}_{\mathbf{p_1}}^{\mathbf{T}}, \mathbf{W}_{\mathbf{p_2}}^{\mathbf{T}} \in \mathbb{R}^{D_h \times \text{half_}hid}$, $\mathbf{b_{p1}} \in \mathbb{R}^{\text{half_}hid}$, $\mathbf{V_p} \in \mathbb{R}^{\text{half_}hid}$, half_ $hid = \left\lfloor \frac{\mathbf{n}_{hidden}}{2} \right\rfloor$ and $b_{pv} \in \mathbb{R}^1$ are trainable parameters. The attention scores form a batched matrix $\mathbf{A}^P \in \mathbb{R}^{B \times N \times N}$ that undergoes L_2 normalization. The batched gating matrix is:

$$\mathbf{G}^* = \operatorname{Sigmoid}(\mathbf{A}^P \mathbf{W_b} + w_b) \tag{39}$$

where $\mathbf{W_b} \in \mathbb{R}^{N \times N}$, $w_b \in \mathbb{R}$, are trainable parameters yielding $\mathbf{G}^* \in \mathbb{R}^{B \times N \times N}$. The dynamic adjacency is:

$$\mathbf{A_{dynamic}} = (\mathbf{A}^G \odot \mathbf{G}^*) + (\mathbf{A}^P \odot (1 - \mathbf{G}^*)) \in \mathbb{R}^{B \times N \times N}$$
(40)

where $\mathbf{A}^G = \text{Expand}(\tilde{\mathbf{A}}^{geo}) \in \mathbb{R}^{B \times N \times N}$ is the batched normalized geographical adjacency matrix.

- EpiGNN-style Spatial Adjacency:

The degree vector $\mathbf{d} \in \mathbb{R}^{N \times 1}$ is expanded to Expand $(\mathbf{d}) \in \mathbb{R}^{B \times N \times 1}$. The gating term is:

$$\mathbf{D_{mat}} = \operatorname{Sigmoid}(\mathbf{W}^{gate} \odot (\operatorname{Expand}(\mathbf{d})\operatorname{Expand}(\mathbf{d})^{T})) \tag{41}$$

where $\mathbf{W}^{gate} \in \mathbb{R}^{N \times N}$, Expand(d)Expand(d)^T $\in \mathbb{R}^{B \times N \times N}$, yielding $\mathbf{D}_{mat} \in \mathbb{R}^{B \times N \times N}$. The spatial adjacency is obtained by:

$$\tilde{\mathbf{A}}_{spatial} = \mathbf{D}_{mat} \odot \mathbf{A}^G \in \mathbb{R}^{B \times N \times N}$$
(42)

- Final Fusion:

$$\tilde{\mathbf{A}}_{Hybrid} = \mathbf{A}_{\mathbf{dynamic}} + \tilde{\mathbf{A}}_{spatial} + \tilde{\mathbf{A}}^{e'}$$
(43)

Here, $\tilde{\mathbf{A}}^{e'} = \operatorname{Expand}(\mathbf{A}^{e'}) \in \mathbb{R}^{B \times N \times N}$ is the batched external relation matrix. Finally, convert $\tilde{\mathbf{A}}_{Hybrid}$ to its corresponding Laplacian matrix $\mathbf{L}^{lapl} \in \mathbb{R}^{B \times N \times N}$, as input to the GNN layers.

• Feature Fusion and Graph Message Passing (GCN Layers)

– Initial Node Feature Fusion $(H_0^{(0)})$

Before graph message passing, concatenate the features extracted from various modules to form the initial node feature vector for the GNN. These features include: multi-scale temporal features $\tilde{\mathbf{H}}^C$, local transmission risk $\mathbf{H_{ltr}}$ and global transmission risk $\mathbf{H_{gtr}}$.

$$\mathbf{H_0^{(0)}} = \operatorname{Concat}(\tilde{\mathbf{H}}^C, \mathbf{H_{ltr}}, \mathbf{H_{gtr}}) \in \mathbb{R}^{B \times N \times (D_c + 2hidR)}$$
(44)

- Multi-layer GCN Propagation:

Use $\mathbf{H_0^{(0)}}$ as input, propagating through several graph convolutional layers. Each graph convolutional layer aggregates neighbor information and transforms node features under the guidance of the dynamic Laplacian matrix \mathbf{L}^{lapl} .

$$\tilde{\mathbf{H}}^{(l+1)} = \text{LayerNorm}(\text{ReLU}(\mathbf{L}^{lapl}\tilde{\mathbf{H}}^{(l)}\tilde{\mathbf{W}}^{(l)}))$$
(45)

Here, $\tilde{\mathbf{W}}^{(l)} \in \mathbb{R}^{(D_c+2hidR)\times(D_c+2hidR)}$ is a weight matrix, $\tilde{\mathbf{H}}^{(l)} \in \mathbb{R}^{B\times N\times(D_c+2hidR)}$ is the node representation at l_{th} layer. LayerNorm(·) is layer normalization operation, which helps stabilize training. The final GCN output is $\tilde{\mathbf{H}}_{GCN} \in \mathbb{R}^{B\times N\times D_{gcn}}$. If residual connections are enabled, $D_{gcn} = (n_{gcn}+1)(D_c+2hidR)$, where n_{gcn} is the number of GCNs; otherwise, $D_{gcn} = D_c + 2hidR$.

• Prediction (Ŷ)

The final prediction input consists of two concatenated parts: the final node features $\tilde{\mathbf{H}}_{GCN}$ learned by the GCN, which contain spatio-temporal information, and the pure temporal hidden states $\tilde{\mathbf{H}}_{RNN}$ extracted by the RNN. The concatenated features are fed into a linear layer, mapping them to the final prediction dimension.

$$\mathbf{res} = \operatorname{Linear}_{output}(\operatorname{Concat}(\tilde{\mathbf{H}}_{GCN}, \tilde{\mathbf{H}}_{RNN})) \tag{46}$$

Linear_{output} maps $\mathbb{R}^{D_{gcn}+D_h} \to \mathbb{R}^1$, yielding $\mathbf{res} \in \mathbb{R}^{B \times N}$. Furthermore, if a residual window is configured, the model will also add a direct residual connection $\mathbf{P_t}$:

$$\mathbf{P_t} = \operatorname{Linear}_{residual}(\operatorname{Flatten}(\tilde{\mathbf{X}}_{e'}, [:, -\operatorname{residual_window}:, :])) \tag{47}$$

The residual term \mathbf{P}_t is computed by flattening the most recent residual_window time steps of input $\tilde{\mathbf{X}}_{e':} \in \mathbb{R}^{B \times T \times N}$ (sliced as $\mathbf{X}[:, -\text{residual_window}:,:] \in \mathbb{R}^{B \times \text{residual_window} \times N}$) into $\mathbb{R}^{(B \cdot N) \times \text{residual_window}}$, then applying the linear transformation Linear_residual to project it to $\mathbb{R}^{(B \cdot N) \times 1}$, which is ultimately reshaped into the final residual output $\mathbf{P}_t \in \mathbb{R}^{B \times N}$ for element-wise combination with the main prediction.

The final prediction $\hat{\mathbf{Y}}$ is a combination of the linear layer output **res** and the residual term $\mathbf{P_t}$:

$$\hat{\mathbf{Y}} = \mathbf{res} \cdot \text{ratio} + \mathbf{P_t} \in \mathbb{R}^{B \times N}$$
(48)

where ratio is an adjustable weight parameter. The loss function for this model remains the same as that of the ColaGNN model.

6.4 Experiments and Analysis

6.4.1 Comparison with State-of-the-art

This section is about the second set of experiments, which evaluate the performance of our proposed HybridGNN against a diverse set of state-of-the-art baseline models on four datasets: Australia-COVID, US-Regions, US-States, and Japan-Prefectures. These baselines comprise three Graph Neural Network (GNN) models (EpiGNN, ColaGNN, and STGCN), two traditional time series models (GAR and VAR), and two deep learning models (LSTM and CNNRNN-Res). We compare their prediction accuracy using MAE, RMSE, and PCC metrics, with HybridGNN demonstrating consistent superiority across these diverse benchmarks. It is important to note that for the second set of experiments, the hyperparameter settings and environmental configurations for all models (including EpiGNN, ColaGNN, and STGCN from the first experiment, as well as the newly introduced baselines) remain consistent with those established in the first experiment, ensuring a fair and comparable evaluation.

The selected baseline models are described as follows:

- **EpiGNN**: As a foundational component of our proposed HybridGNN, EpiGNN is an innovative graph neural network that integrates an autoregressive (AR) component with graph convolution.
- ColaGNN: Also a key component of our proposed HybridGNN, ColaGNN is another specialized graph neural network for epidemic prediction. It primarily leverages an attention mechanism to model complex cross-regional influences.
- STGCN (Spatiotemporal Graph Convolutional Network): A classic and widely used spatiotemporal graph neural network. It effectively processes data with complex spatiotemporal dependencies by combining Graph Convolution with Gated Recurrent Units (GRUs).
- GAR (Global Autoregression): A classical statistical time series model that models the current value of a variable based on its own past values, often applied globally across all regions or an aggregated series.
- VAR (Vector Autoregression): A classical multivariate time series statistical model. It predicts future values by establishing linear relationships between current observations and lagged observations of itself and other variables.
- LSTM (Long Short-Term Memory)[16]: A widely used variant of Recurrent Neural Networks (RNNs), adept at processing and predicting long-term dependencies in time series data.
- CNNRNN-Res (Convolutional Neural Network-Recurrent Neural Network with Residual Connections)[7]: A model that combines Convolutional Neural Networks (CNNs) and Recurrent Neural Networks (RNNs), incorporating residual connections to enhance training stability and performance.

Next, we will proceed with a detailed analysis of the experimental results, delving into the specific performance of our proposed HybridGNN across different datasets, prediction metrics, and prediction horizons.

• Australia-COVID Dataset Prediction Analysis (daily)

Dataset						Australi	a horizon					
Method	Metric	2	5	8	11	14	17	20	23	26	29	32
	MAE	127.2462	124.4751	100.5464	112.6527	163.1471	170.5775	194.5076	212.0276	210.8035	281.8333	304.4768
EpiGNN	RMSE	388.4988	341.1904	315.3492	370.0045	495.6291	513.5239	573.4510	617.0450	614.6236	725.7447	828.0177
	PCC	0.9942	0.9925	0.9919	0.9905	0.9887	0.9864	0.9863	0.9840	0.9810	0.9816	0.9834
	MAE	38.5352	68.9650	117.7698	129.8169	149.3325	154.6378	116.4481	142.1623	145.5120	129.1289	108.8203
ColaGNN	RMSE	180.3111	276.6119	434.2820	458.9208	523.0732	546.5959	450.7830	513.2499	547.5039	499.4233	430.2485
	PCC	0.9974	0.9948	0.9882	0.9878	0.9828	0.9798	0.9833	0.9798	0.9747	0.9781	0.9841
	MAE	451.3148	229.8330	295.4140	335.3027	305.1303	268.4486	679.8415	190.1576	245.7612	268.5856	413.9621
STGCN	RMSE	1052.6590	601.9303	796.3123	911.3586	842.0427	723.1620	1837.4347	572.1667	716.6028	683.0385	919.0851
	PCC	0.8412	0.9829	0.9622	0.9763	0.9835	0.9850	0.8897	0.9833	0.9818	0.9743	0.8863
	MAE	23.4004	31.4465	59.6352	61.4129	67.5602	68.4927	74.4453	64.4795	81.6012	80.8418	75.6295
Hybrid	RMSE	116.4416	164.0043	222.4653	268.5012	280.7851	288.4950	322.6047	308.9084	329.5613	331.7577	337.1171
	PCC	0.9988	0.9971	0.9956	0.9907	0.9898	0.9893	0.9871	0.9895	0.9859	0.9859	0.9860
	MAE	8.9417	15.1683	79.1240	148.9641	264.6193	134.7348	184.2222	184.7187	184.2292	183.7146	182.5061
GAR	RMSE	40.1244	69.8092	241.3218	433.3076	750.3112	405.9869	412.4550	417.0376	420.3875	422.8731	424.9285
	PCC	0.9998	0.9995	0.9985	0.9974	0.9958	0.9807	0.9800	0.9795	0.9792	0.9789	0.9787
	MAE	157.4892	188.9837	165.8157	157.3335	150.6911	141.9377	138.8578	131.7199	134.7356	137.5603	139.8792
VAR	RMSE	456.6433	489.5019	489.8395	442.9908	437.2672	417.8038	407.6312	388.0964	386.1478	394.1534	396.2959
	PCC	0.9725	0.9679	0.9680	0.9737	0.9744	0.9767	0.9779	0.9800	0.9805	0.9802	0.9798
	MAE	32.0964	31.8847	78.7997	211.0995	153.1046	143.2282	132.6313	522.4177	567.1666	606.9993	661.5128
LSTM	RMSE	169.4802	179.0023	280.9579	685.5695	563.6907	528.0544	485.7819	1458.4171	1573.6785	1678.5492	1856.1701
	PCC	0.9974	0.9964	0.9953	0.9776	0.9779	0.9803	0.9841	0.9891	0.9855	0.9796	0.9744
	MAE	499.0875	121.5019	125.1909	115.6163	122.2715	170.9541	194.8863	226.9638	240.5815	242.1965	241.9350
${\rm CNNRNN\text{-}Res}$	RMSE	1242.8349	358.7626	377.3631	384.8045	407.0471	515.7392	578.3274	562.5536	593.0843	599.3848	605.8610
	PCC	0.9559	0.9900	0.9883	0.9872	0.9856	0.9838	0.9838	0.9753	0.9743	0.9741	0.9751

Table 6: Performance Comparison of All Prediction Models on Australia-COVID Dataset with Horizon = 2, 5, 8, 11, 14, 17, 20, 23, 26, 29, 32. The underlined indicates the second-best, and bold indicates the best.

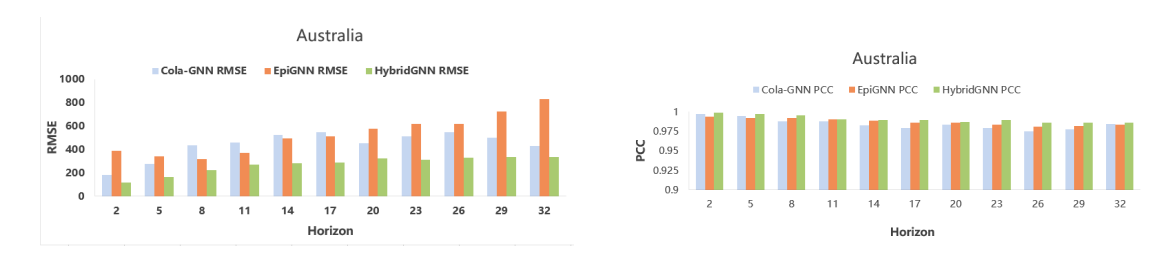


Figure 8: Performance Comparison between HybridGNN and two baselines (EpiGNN and ColaGNN) on Australia-COVID dataset

The HybridGNN model demonstrates outstanding performance on the Australia dataset. Compared to the fusion models EpiGNN and ColaGNN, HybridGNN consistently achieves lower MAE and RMSE values, along with higher PCC scores, indicating superior prediction accuracy and stronger correlation with real-world data, which is illustrated in Figure 8. Furthermore, when measured against all other models in the Table 6 (including STGCN, GAR, VAR, LSTM, and CNNRNN-Res), HybridGNN maintains the lowest MAE and RMSE values across almost all horizons, while also securing the leading position in PCC. This unequivocally highlights HybridGNN's exceptional predictive capabilities and stability on the Australia dataset.

• US-Regions Dataset Prediction Analysis (weekly)

Dataset				Japan					$\operatorname{US-Regions}$					US-States		
Dutane				horizon					horizon					horizon		
Method	Metric	2	5	14	23	29	2	5	14	23	29	2	5	14	23	29
EpiGNN	MAE RMSE PCC	$\begin{array}{c} 317.7547 \\ \underline{934.0154} \\ 0.9168 \end{array}$	421.4113 1051.202 0.9016	532.3716 1466.451 0.7321	580.0948 1403.616 0.7966	572.4716 1551.241 0.722	271.9734 495.2303 0.9421	543.7277 898.0375 0.7813	584.1873 994.9219 0.7312	743.6681 1203.012 0.5585	679.3557 1043.007 0.6884	58.6324 148.2381 0.9449	85.646 199.371 0.8975	$\frac{107.6102}{228.3557}\\0.8601$	108.9413 236.3079 0.8508	138.4842 265.86 0.8088
ColaGNN	MAE RMSE PCC	287.5924 948.7436 0.9253	379.4594 1152.288 0.8628	$\frac{491.446}{1412.874}$ $\underline{0.7812}$	499.7023 1383.584 0.8098	492.9672 1540.414 0.6967	233.6242 506.9187 0.9435	525.8035 1007.584 0.7988	708.7531 1260.498 <u>0.6874</u>	$\frac{658.7186}{1061.498}$ $\frac{0.6701}{}$	484.4075 969.8692 0.774	53.4726 148.1823 <u>0.9498</u>	83.3606 221.7605 0.8747	95.2117 229.4957 0.8797	101.7764 238.5425 0.8663	$\frac{102.4193}{233.7741}$ $\underline{0.8613}$
STGCN	MAE RMSE PCC	304.3613 967.6338 0.9071	433.1643 1301.511 0.8382	538.246 1598.077 0.7752	568.3075 1434.441 0.7725	518.1366 1455.733 0.8322	408.5528 697.2763 0.8783	556.1506 1066.68 0.7682	800.3231 1381.32 0.4352	768.8422 1305.12 0.5499	587.5015 1077.738 0.7464	82.7078 181.8974 0.914	101.3556 235.4713 0.8517	112.4669 271.1715 0.8092	111.9671 254.2331 0.8281	108.3811 244.7531 0.8453
HybridGNN	MAE RMSE PCC	270.804 921.458 0.9217	$\begin{array}{r} {\bf 379.3438} \\ {\underline {1121.055}} \\ {\underline {0.8847}} \end{array}$	486.6925 1408.038 0.7848	470.0945 1319.952 0.8252	479.2033 1410.298 <u>0.7812</u>	227.9353 493.3472 0.9464	434.3308 833.6702 0.8321	658.3672 1157.178 0.6504	590.7435 993.2136 0.7408	449.7577 890.3559 0.7988	52.0503 137.7529 0.9547	76.3155 196.3588 0.9058	100.0204 225.7914 0.8663	99.3903 220.7136 0.8764	101.9999 226.6243 0.8713
GAR	MAE RMSE PCC	348.4744 1229.896 0.8049	636.3506 1976 0.3494	698.4774 2021.932 0.4629	698.1638 2029.766 0.4532	598.0141 1726.18 0.5547	261.3882 542.1134 0.9319	525.5662 1000.35 0.7919	848.754 1488.593 0.5115	750.9815 1338.422 0.5285	552.1652 1027.191 0.7468	55.9509 149.855 0.9438	93.999 234.4273 0.8745	144.8457 340.4244 0.7435	138.0241 330.7043 0.7458	120.9852 285.3659 0.7911
VAR	MAE RMSE PCC	511.1963 1365.755 0.7496	770.097 2032.304 0.2849	746.0118 1900.42 0.4814	802.3989 1895.832 0.45	676.3038 1714.732 0.564	420.2119 727.6051 0.683	626.335 1047.776 0.6942	828.1846 1318.061 0.4577	784.1926 1264.515 0.5543	638.3933 1081.703 0.6698	111.8088 228.0389 0.8619	130.3733 279.3023 0.7884	160.3149 337.2174 0.6994	179.0292 382.3912 0.6216	153.7718 320.2148 0.7252
LSTM	MAE RMSE PCC	274.2626 968.1576 0.9037	399.1941 1181.527 0.8614	536.7787 1599.631 0.7312	551.9538 1390.769 0.7525	510.3136 1530.291 0.7573	243.4456 528.9254 0.9397	485.064 972.9679 0.8207	760.6742 1231.165 0.5282	736.6856 1204.848 0.5659	741.2546 1206.959 0.5626	52.3984 144.6276 0.948	78.9112 207.0022 0.8932	125.9012 300.834 0.7619	145.2799 341.6578 0.7328	147.0832 343.9574 0.7301
CNNRNN-Res	MAE RMSE PCC	337.4548 1063.797 0.8606	661.3301 1984.306 0.3336	745.3217 2110.505 0.1309	910.321 1960.829 0.3112	617.5538 1672.761 0.6858	317.7955 588.6313 0.9177	499.8897 926.6054 0.787	795.5295 1299.886 0.4575	720.0831 1257.29 0.5504	855.8668 1483.717 0.4687	93.2001 215.2229 0.8817	107.1022 258.2973 0.8343	111.1416 262.0959 0.821	108.3219 273.2706 0.8429	108.1891 258.789 0.8436

Table 7: Performance comparison across three datasets with representative horizons: short-term (2,5), mid-term (14), and long-term (23,29)

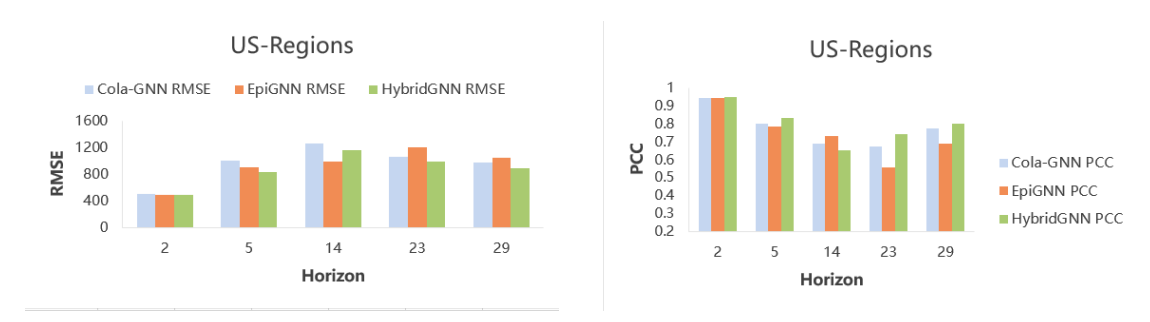


Figure 9: Performance Comparison between HybridGNN and two baselines (EpiGNN and ColaGNN) on US-Regions dataset

On the US-Regions dataset, the HybridGNN model demonstrates significant performance advantages, as is shown in Table 7 and further illustrated in Figure 9. Compared to the fusion models EpiGNN and ColaGNN, HybridGNN consistently achieves lower MAE and RMSE values across most prediction horizons, and generally higher PCC values. This indicates its predictions are more accurate and show a stronger correlation with actual data, although EpiGNN was slightly superior in MAE and RMSE at horizon 14, and ColaGNN also slightly better in MAE at that same horizon. When considering all models, HybridGNN largely stands out with the lowest MAE and RMSE values and leading PCC scores across various time steps, fully proving its excellent predictive performance and stability on the US-Regions dataset.

• US-States Dataset Prediction Analysis (weekly)

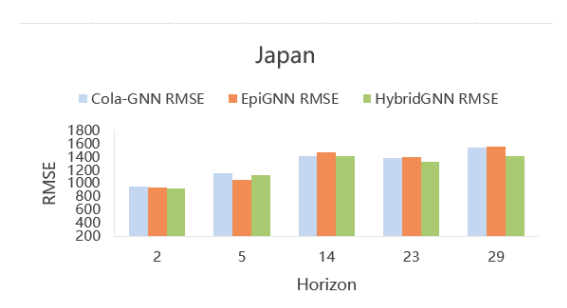




Figure 10: Performance Comparison between HybridGNN and two baselines (EpiGNN and ColaGNN) on US-States dataset

On the US-States dataset, the HybridGNN model demonstrates consistently superior overall performance, which is detailed in Table 7 and further illustrated in Figure 10. It achieves the lowest RMSE values across all time horizons, significantly outperforming all comparative models, including the fusion models EpiGNN and ColaGNN. This indicates its predictions have the smallest error margins. For MAE and PCC, HybridGNN also generally performs best across most prediction periods, yielding the lowest MAE and highest PCC values. The only exception is at horizon 14, where ColaGNN shows slightly better performance in both MAE and PCC. Overall, HybridGNN's notable advantages in error control and data correlation prove its strong predictive capabilities on the US-States dataset.

• Japan-Prefectures Dataset Prediction Analysis (weekly)



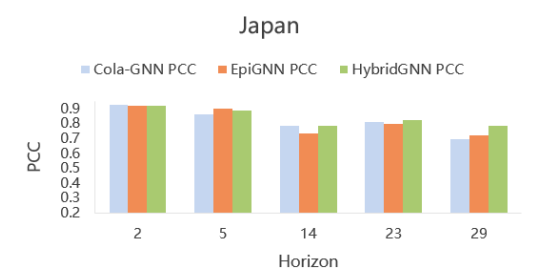


Figure 11: Performance Comparison between HybridGNN and two baselines (EpiGNN and ColaGNN) on Japan-Prefectures dataset

The analysis is detailed in Table 7 and further illustrated in Figure 11. On the Japan-Prefectures dataset, the HybridGNN model demonstrates remarkably superior overall performance. Compared to the fusion models EpiGNN and ColaGNN, HybridGNN achieves the best MAE across all time horizons and leads in RMSE for most horizons, indicating significantly higher prediction accuracy than both. While ColaGNN and EpiGNN show slightly better PCC in some short-term predictions (e.g., horizons 2 and 5), HybridGNN performs best in PCC for mid-to-long-term forecasts (horizons 14 and 23). When compared against all other models, HybridGNN's universal leadership in MAE and its majority advantage in RMSE highlight its robust error control capabilities, making it the most outstanding model on this dataset, with other models (like STGCN at horizon 29) only marginally excelling in isolated PCC metrics.

Summary: Overall, our proposed HybridGNN demonstrates significant and often superior performance across the evaluated datasets. Its superiority is most pronounced on the Australia-COVID and US-States datasets, where it consistently achieves the best RMSE and PCC across almost all prediction horizons. This demonstrates the powerful synergy achieved by combining the complementary strengths of EpiGNN and ColaGNN. On the US-Regions dataset, HybridGNN again proves to be the most robust model, delivering the lowest error in the crucial long-term stages and effectively balancing short-term accuracy with long-term stability. Crucially, on the highly volatile Japan-Prefectures dataset, HybridGNN delivers a highly competitive and often superior performance. It secures the lowest error at multiple key horizons, showcasing its robustness and adaptability even in complex, high-volatility scenarios. In conclusion, HybridGNN establishes itself not just as a general and robust model, but as a top-tier performer for epidemic forecasting, demonstrating its potential by excelling in both stable and highly challenging environments.

6.4.2 Ablation Tests

To analyze the effect of each component in our framework, we perform ablation tests with the following settings:

- Hybrid w/o ctemp: Removes Conv1D to capture short-term and long-term temporal dependencies, but instead uses a simple linear layer to process the raw time-series input as node features.
- Hybrid w/o LTR: Removes the local transmission risk encoding module. This means
 that the node feature H_{ltr} will not be concatenated into the GNN's input during the feature
 fusion stage.
- Hybrid w/o GTR: Removes the global transmission risk encoding module. This means that the node feature \mathbf{H}_{gtr} will not be concatenated into the GNN's input during the feature fusion stage.
- Hybrid w/o dygraph: Removes ColaGNN-style dynamic graph. In this case, the model
 only uses the static geographical adjacency matrix combined with degree information to
 construct the final adjacency matrix, without employing the RNN-based dynamic attention
 mechanism.

RMSE	2	5	8	11	14	17	20	23	26	29	32
					Australia						
Hybrid w/o ctemp	415.9470	1991.1867	11594.0336	433.4485	1916.5805	1931.0230	1956.7124	1974.4552	1874.6233	1902.2566	1975.7156
Hybrid w/o LTR	273.6972	356.7588	381.4664	451.2182	696.5153	1178.9851	1138.2398	1418.4840	1385.6420	1506.8618	1595.1749
Hybrid w/o GTR	243.9937	287.4677	356.9107	326.7577	820.5287	964.1199	1145.3360	1393.4021	1450.5515	1528.8793	1591.1614
Hybrid w/o dygraph	1912.3533	1961.3242	1998.8525	2032.4530	2036.5009	2034.0261	2032.8792	2006.7390	2010.6395	2019.1537	2028.1556
Hybrid	116.4416	164.0043	222.4653	268.5012	280.7851	288.4950	322.6047	308.9084	329.5613	331.7577	337.1171
					$US ext{-}States$						
Hybrid w/o ctemp	147.8191	218.4046	232.9632	270.1645	243.2812	322.0208	332.0216	292.4265	271.2481	252.0407	248.6336
Hybrid w/o LTR	144.2372	216.5336	239.4663	252.3514	227.7764	245.1995	260.3577	289.3448	224.8867	254.3987	237.0310
Hybrid w/o GTR	141.4485	206.0671	232.3240	241.0928	229.4291	242.5869	246.6565	248.1291	261.1806	246.2272	246.9301
Hybrid w/o dygraph	191.5346	227.8267	253.8217	254.7951	252.8139	251.5027	246.1103	242.6997	248.6554	256.4419	254.6796
Hybrid	137.7529	196.3538	231.9247	235.4558	225.7914	235.5321	220.5349	220.7136	231.0958	226.6243	234.6385

Table 8: RMSE Performance of HybridGNN Variants in Ablation Study on Australia and US-States Datasets (Lower is better)

The results for RMSE are shown in the Table 8. We observe that:

- Overall Trend: In most cases, the full model (Hybrid) performs optimally in terms of RMSE, especially on the Australia dataset, where its RMSE values are significantly lower than all ablation variants. This indicates that all components work collaboratively to effectively reduce prediction error.
- Importance of Temporal Features (Hybrid vs Hybrid w/o ctemp): On the Australia dataset, removing temporal features (Hybrid w/o ctemp) leads to a significant increase in RMSE, particularly for short-term predictions (e.g., 2, 5, 8, 11), sometimes by orders of magnitude worse than other ablated models. This highlights the critical role of temporal feature extraction in capturing Australian influenza trends. On the US-States dataset, removing temporal features also generally increases RMSE, though not as drastically as for Australia.
- Importance of Global Transmission Risk (Hybrid vs Hybrid w/o GTR): Removing GTR (Hybrid w/o GTR) generally leads to an increase in RMSE. On the Australia dataset, the presence of GTR significantly reduces RMSE for both short-term and long-term predictions. On the US-States dataset, GTR also plays a key role in reducing RMSE at multiple time steps (e.g., 11, 17).
- Importance of Local Transmission Risk (Hybrid vs Hybrid w/o LTR): Removing LTR (Hybrid w/o LTR) also generally leads to an increase in RMSE. On the Australia dataset, LTR's contribution to RMSE reduction is similar to GTR's. On the US-States dataset, LTR has a noticeable impact on some short-term and long-term predictions (e.g., 2, 23, 32), but is not as universally beneficial as GTR.
- Importance of Dynamic Graph (Hybrid vs Hybrid w/o dygraph): Removing the dynamic graph (Hybrid w/o dygraph) leads to a substantial degradation in RMSE on the Australia dataset, indicating that the dynamic graph is crucial for capturing complex interregional relationships. On the US-States dataset, while also degraded, the magnitude is less severe than for Australia, which might suggest the initial importance of geographical structure in the US dataset.

PCC	2	5	8	11	14	17	20	23	26	29	32
				I	Australia						
Hybrid w/o ctemp	0.9859	0.2674	0.0291	0.9898	0.3228	0.2412	0.2461	0.1803	0.3199	0.3595	0.1857
Hybrid w/o LTR	0.9945	0.9935	0.9924	0.9910	0.9890	0.9837	0.9847	0.9795	0.9816	0.9757	0.9753
Hybrid w/o GTR	0.9959	0.9956	0.9936	0.9883	0.9900	0.9876	0.9852	0.9840	0.9807	0.9796	0.9772
Hybrid w/o dygraph	0.3523	0.3686	0.3477	0.2833	0.2892	0.3593	0.3496	0.3780	0.3916	0.3848	0.3577
Hybrid	0.9988	0.9971	0.9956	0.9950	0.9898	0.9893	0.9871	0.9895	0.9859	0.9856	0.9860
				U	S-States						
Hybrid w/o ctemp	0.9485	0.8847	0.8741	0.8185	0.8643	0.7640	0.7220	0.7900	0.8129	0.8302	0.8385
Hybrid w/o LTR	0.9526	0.8891	0.8536	0.8417	0.8672	0.8557	0.8594	0.8267	0.8716	0.8404	0.8495
Hybrid w/o GTR	0.9528	0.9033	0.8752	0.8626	0.8779	0.8690	0.8596	0.8663	0.8474	0.8434	0.8416
Hybrid w/o dygraph	0.9039	0.8630	0.8319	0.8356	0.8321	0.8467	0.8509	0.8452	0.8439	0.8314	0.8271
Hybrid	0.9547	0.9058	0.8633	0.8635	0.8663	0.8511	0.8730	0.8746	0.8746	0.8713	0.8505

Table 9: PCC Performance of HybridGNN Variants in Ablation Study on Australia and US-States Datasets (Higher is better)

The results for PCC are shown in the Table 9. We observe that:

• Overall Trend: The full model (Hybrid) performs best in terms of PCC, especially on the Australia dataset, where its PCC values are generally the highest, close to 1. This indicates that the complete model excels at capturing the linear relationship between predictions and true values.

- Importance of Temporal Features (Hybrid vs Hybrid w/o ctemp): Removing temporal features (Hybrid w/o ctemp) leads to a significant drop in PCC. On the Australia dataset, some PCC values become very low (close to 0), demonstrating a loss of ability to capture sequence trends. This again emphasizes the necessity of temporal feature extraction.
- Importance of Global Transmission Risk (Hybrid vs Hybrid w/o GTR): Removing GTR (Hybrid w/o GTR) generally leads to a decrease in PCC. On the Australia dataset, although it performs sub-optimally at certain time steps (e.g., 8, 11, 14), overall it does not match the performance of the full model. On the US-States dataset, GTR's contribution to PCC improvement is significant at several time steps (e.g., 8, 11, 14, 17).
- Importance of Local Transmission Risk (Hybrid vs Hybrid w/o LTR): Removing LTR (Hybrid w/o LTR) also generally leads to a decrease in PCC. On the Australia dataset, LTR's contribution to PCC is similar to GTR's. On the US-States dataset, LTR performs exceptionally well at some time steps (e.g., 32), even outperforming the full model, but is less effective at others.
- Importance of Dynamic Graph (Hybrid vs Hybrid w/o dygraph): Removing the dynamic graph (Hybrid w/o dygraph) results in a significant drop in PCC on both datasets, especially on the Australia dataset where PCC values become very low, reiterating the crucial role of the dynamic graph in modeling complex spatial dependencies.

In summary, the table data strongly demonstrates the importance of temporal feature extraction, global transmission risk encoding, local transmission risk encoding, and dynamic graph construction components within the HybridGNN model for improving prediction accuracy and correlation. Specifically, temporal features and the dynamic graph are crucial for the model's robustness and performance, and these modules show greater advantage in long-term predictions.

6.4.3 Sensitivity Analysis

Look-back Window	US-States	Australia	US-Regions	Japan
	RMSE / PCC	RMSE / PCC	$\overline{\mathbf{RMSE} / \mathbf{PCC}}$	RMSE / PCC
10	328.5342 / 0.7433	901.5119 / 0.9902	1266.6971 / 0.4745	1791.2859 / 0.6202
20	237.8147 / 0.8458	298.4658 / 0.9894	1431.4211 / 0.4757	1539.2149 / 0.7511
30	235.0392 / 0.8836	546.33 / 0.9913	1000.9503 / 0.783	1749.5062 / 0.6332
40	251.5761 / 0.8702	452.632 / 0.9915	963.2282 / 0.74	$1399.8574 \; / \; 0.8072$
50	225.6077 / 0.8765	842.7432 / 0.9899	1107.5108 / 0.6713	1766.8719 / 0.7078

Table 10: Performance Metrics (RMSE and PCC) for Different Look-back Windows (horizon=15)

#Filter	US-States	Australia	US-Regions	Japan
	MAE / RMSE	MAE / RMSE	$\mathbf{MAE} \ / \ \mathbf{RMSE}$	$\mathbf{MAE} \ / \ \mathbf{RMSE}$
4	115.8689 / 257.4315	175.8813 / 514.0602	678.907 / 1235.6178	594.0095 / 1701.2319
8	107.9496 / 237.9043	$73.2646 \; / \; 280.7642$	813.9878 / 1431.4215	585.1898 / 1580.785
16	$101.8772 \; / \; 237.2356$	173.789 / 529.2308	765.532 / 1353.777	770.1307 / 1689.6497
32	$134.9709 \ / \ 313.0276$	295.3007 / 836.9718	783.0477 / 1326.0179	576.2716 / 1710.5112
64	$108.1324 \ / \ 254.8871$	$196.1771 \ / \ 562.5098$	$782.9492 \ / \ 1337.6009$	$604.6296 \ / \ 1705.8411$

Table 11: Performance Metrics (MAE and RMSE) for Different Filter Numbers (horizon=15)

Learning Rate	US-States	Australia	US-Regions	Japan
	MAE / RMSE	MAE / RMSE	MAE / RMSE	MAE / RMSE
0.001	107.9496 / 237.9043	73.2646 / 280.7642	813.9878 / 1431.4215	585.1898 / 1580.785
0.005	98.1949 / 223.8596	70.1162 / 275.4259	$748.0739 \; / \; 1250.8788$	518.6663 / 1513.5086
0.01	113.3158 / 276.8495	55.2511 / 276.8183	761.1348 / 1305.3237	511.2254 / 1457.708

Table 12: Performance Metrics (MAE and RMSE) for Different Learning Rates (horizon=15)

RNN Dimension	US-States	${f Australia}$	US-Regions	Japan
	$\overline{\text{MAE} / \text{RMSE}}$	$\overline{\text{MAE} / \text{RMSE}}$	$\overline{\text{MAE} / \text{RMSE}}$	$\overline{\text{MAE} / \text{RMSE}}$
10	135.515 / 300.9511	293.4158 / 830.2479	788.5283 / 1381.8195	666.9337 / 1860.412
20	109.5947 / 239.8612	68.1439 / 300.171	813.9877 / 1431.4214	599.566 / 1606.8013
30	105.7395 / 235.3523	88.8185 / 365.8249	722.9141 / 1265.7188	778.213 / 1749.8347
40	118.7727 / 263.5005	90.3212 / 291.4734	762.4515 / 1325.7405	574.501 / 1620.651
50	106.0453 / 233.0153	67.6961 / 313.1836	738.3013 / 1319.2782	565.5046 / 1601.9304

Table 13: Performance Metrics (MAE and RMSE) for Different RNN Dimensions (horizon=15)

This section evaluates the robustness of the model's performance with respect to key hyperparameters, including the look-back window, number of filters, learning rate, and RNN dimension. The analysis leverages RMSE, PCC (for look-back window experiments), and MAE (for other cases) as primary metrics, applied to four distinct datasets: US-States, Australia-COVID, US-Regions, and Japan-Prefectures. All experiments maintain a consistent horizon of 15.

- Variation in Look-back Window To evaluate the model's reliance on the extent of historical data, we tested look-back windows at intervals of 10, 20, 30, 40, and 50. In Table 10, for US-States, RMSE fluctuates between 225.6077 and 328.5342, with the lowest value at 50, and PCC ranges from 0.7433 to 0.8836, peaking at 30, suggesting a degree of resilience to window size changes. Australia displays a wider RMSE spread (298.4658 to 901.5119), with the best outcome at 20, and PCC values remaining consistently high (0.9894 to 0.9915), pointing to notable sensitivity. US-Regions achieves its minimum RMSE at 40 (963.2282, PCC 0.74), while Japan optimizes at 40 (RMSE 1399.8574, PCC 0.8072), with a moderate range. The significant RMSE variation in Australia (603.0461) suggests a strong influence from this parameter, likely tied to underlying data characteristics.
- Adjustment of Filter Count The model incorporates a convolutional layer to process time series data, where the number of filters plays a role in feature extraction. We experimented with filter counts of 4, 8, 16, 32, and 64, with performance metrics detailed in Table 11. US-States records its lowest RMSE at 16 filters (237.2356, MAE 101.8772), while Australia performs best at 8 (RMSE 280.7642, MAE 73.2646). US-Regions shows an optimal RMSE at 4 filters (1235.6178, MAE 678.907), and Japan at 32 (RMSE 1580.785, MAE 576.2716). The RMSE range is most pronounced for Australia (556.2076), indicating high sensitivity, whereas Japan exhibits the smallest variation (129.7262). Performance tends to decline with excessive filters (e.g., 64), hinting at potential overfitting with larger configurations.
- Modification of Learning Rate The learning rate, a fundamental aspect of the training process, was varied across 0.001, 0.005, and 0.01 to assess its impact. Results, presented in Table 12, show US-States achieving the best RMSE at 0.005 (223.8596, MAE 98.1949), with a sensitivity range of 52.9899. Australia displays minimal fluctuation (RMSE 275.4259 to

280.7642), optimizing at 0.01 (RMSE 276.8183, MAE 55.2511). US-Regions peaks at 0.005 (RMSE 1250.8788, MAE 748.0739), and Japan at 0.01 (RMSE 1457.708, MAE 511.2254), with a range of 123.077. The limited variation in Australia (1.9%) contrasts with US-States (23.7%), reflecting differing levels of sensitivity to this parameter.

• Alteration of RNN Dimension The RNN dimension, which affects the richness of hidden state representations, was tested at 10, 20, 30, 40, and 50. Findings, reported in Table 13, indicate US-States reaching its lowest RMSE at 50 (233.0153, MAE 106.0453), Australia at 40 (RMSE 291.4734, MAE 90.3212), US-Regions at 30 (RMSE 1265.7188, MAE 722.9141), and Japan at 50 (RMSE 1601.9304, MAE 565.5046). Australia shows the widest RMSE range (538.7745), suggesting significant responsiveness, while US-Regions has the narrowest (165.7026). This implies that increasing dimensions can enhance performance, though excessive values may lead to overfitting in data-limited scenarios.

Summary and Implications: The hyperparameter analysis highlights varied sensitivities across datasets and parameters. Key insights include:

- Look-back Window: US-States favors 50, Australia 20, and US-Regions and Japan 40. A window range of 20–50 is recommended to balance accuracy and efficiency.
- Filter Count: Optimal at 16 (US-States), 8 (Australia), 4 (US-Regions), and 32 (Japan). A moderate count (4–32) is suggested to prevent overfitting.
- Learning Rate: Best at 0.005 (US-States, US-Regions) and 0.01 (Australia, Japan), with a range of 0.005–0.01 proposed for effective training.
- RNN Dimension: Peaks at 50 (US-States, Japan), 40 (Australia), and 30 (US-Regions), with 30–50 advised while monitoring overfitting risks.

6.4.4 Interpretability Analysis

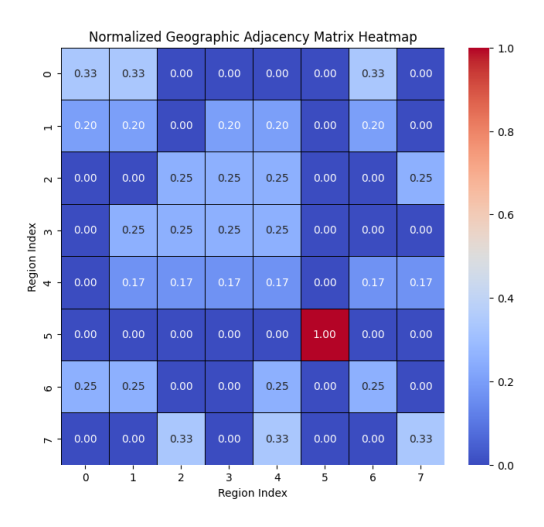
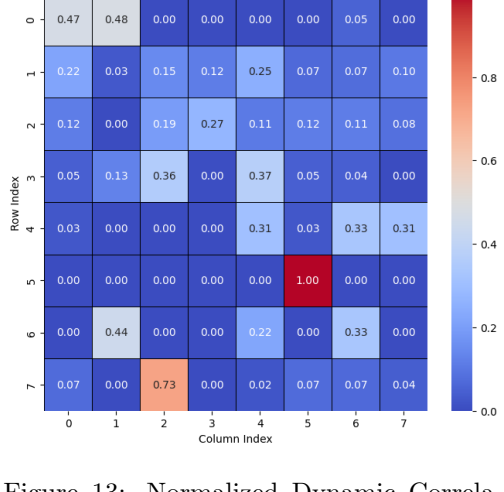


Figure 12: Normalized Geographic Adjacency Matrix Heatmap For Static Propagation



Normalized Dynamic Correlation Matrix Heatmap For EpiGNN

Figure 13: Normalized Dynamic Correlation Matrix Heatmap For EpiGNN

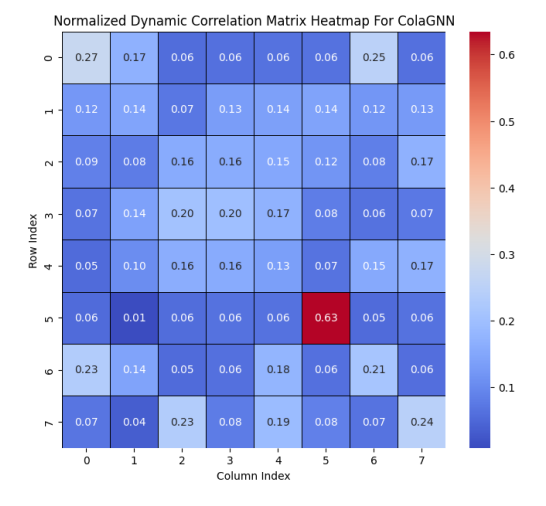


Figure 14: Normalized Dynamic Correlation Matrix Heatmap For ColaGNN

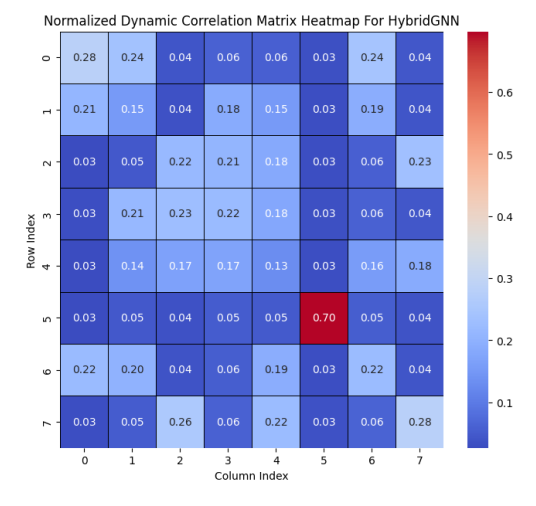


Figure 15: Normalized Dynamic Correlation Matrix Heatmap For HybridGNN

Based on the provided Figures, here is an analysis of why HybridGNN performs better and more stably than the other models on the Australian dataset (e.g., Horizon = 20). These heatmaps compare the performance of four different Graph Neural Network (GNN) models on an Australian dataset by analyzing their normalized correlation matrices. The four figures are:

• Normalized Geographic Adjacency Matrix Heatmap (see Figure 12): This map

shows the region adjacency matrix based on geographic locations. It is obtained by normalizing the matrix \mathbf{A}^{geo} and reflects the physical proximity between regions.

- Normalized Dynamic Correlation Matrix Heatmap For EpiGNN (see Figure 13): This heatmap displays the dynamic correlation matrix for the EpiGNN model, which attempts to capture time-varying interactions between regions.
- Normalized Dynamic Correlation Matrix Heatmap For ColaGNN (see Figure 14): This heatmap shows the dynamic correlation matrix for the ColaGNN model.
- Normalized Dynamic Correlation Matrix Heatmap For HybridGNN (see Figure 15): This heatmap shows the dynamic correlation matrix for the HybridGNN model.

To analyze why HybridGNN's predictions are better and more stable, we need to compare the characteristics of these four heatmaps, especially the differences between HybridGNN and the others. From the heatmaps provided, we can draw the following analysis:

1. Normalized Geographic Adjacency Matrix:

This map (see Figure 12) shows region connectivity based on geographic location. For example, the element at row 5, column 5 is 1.00, indicating a high self-correlation for region 5 (which is expected). Other non-zero values indicate adjacent regions. This matrix is static; it only reflects spatial relationships and does not account for dynamic changes over time.

2. EpiGNN's Dynamic Correlation Matrix:

This map (see Figure 13) displays the dynamic correlations learned by the EpiGNN model, which attempts to capture region connections in dynamic processes like disease spread. Compared to the geographic adjacency matrix, its pattern is different. For instance, the value at row 7, column 2 is 0.73, which is much higher than the corresponding value in the geographic adjacency matrix (0.00). This suggests that EpiGNN might have captured strong correlations between non-geographically adjacent regions. However, the matrix contains many zero values, which could mean the model focuses only on a few strongly correlated regions and ignores other potentially weaker correlations.

3. ColaGNN's Dynamic Correlation Matrix:

This map (see Figure 14) also shows dynamic correlations. Its values are generally smaller, except for row 5, column 5 (0.63). This might indicate that ColaGNN's ability to capture dynamic correlations is relatively weak, or that it distributes weights more evenly across correlations. The value distribution in this matrix appears more uniform than EpiGNN's, with fewer zero values. This could mean it considers more regional relationships but may not highlight the most important ones.

4. HybridGNN's Dynamic Correlation Matrix:

A key feature of this map (see Figure 15) is the high value at row 5, column 5 (0.70), similar to the self-correlation in the geographic adjacency matrix. Compared to the other models' dynamic correlation matrices, HybridGNN's value distribution seems smoother with more non-zero entries. The crucial point is that HybridGNN combines geographic adjacency information with dynamic correlation information. Its matrix pattern might be closer to the geographic adjacency matrix than EpiGNN's, while still incorporating features of dynamic change. For example, its values are generally higher than ColaGNN's, and it doesn't have an excessive number of zeros like EpiGNN.

Comprehensive Analysis and Conclusion:

HybridGNN's superior and more stable performance on the Australian dataset is likely due to its hybrid approach, which effectively integrates static geographic adjacency information with dynamic temporal correlation information.

- Importance of Geographic Adjacency: In prediction tasks like disease spread or traffic flow, geographically adjacent regions often have stronger mutual influences. Ignoring geographic location in favor of only dynamic correlations can cause a model to miss crucial foundational relationships.
- Importance of Dynamic Correlation: Relying solely on a geographic adjacency matrix is static and fails to capture complex interactions that change over time (e.g., shifts in commuting patterns, changes in disease hotspots).
- HybridGNN's Advantage: By combining these two types of information, HybridGNN can capture fundamental spatial dependencies, which are provided by the geographic adjacency matrix. It also can learn dynamic dependencies that change over time, which are provided by the temporal features in the data.

Therefore, the HybridGNN heatmap likely reflects a balance: it is neither a pure geographic adjacency matrix nor a completely random dynamic correlation matrix. It is probably a weighted combination or a clever fusion that better represents the true complex relationships between regions in the Australian dataset, leading to higher accuracy and stability in its predictions.

7 Discussion of the EpiCola-GNN Model

7.1 Strengths of HybridGNN

HybridGNN (EpiCola-GNN) distinguishes itself by merging and extending specific architectural components from both EpiGNN and ColaGNN. This design creates powerful synergies, offering capabilities and performance benefits beyond what its predecessor models can achieve individually.

- Complementary Dynamism: While EpiGNN's GraphLearner generates a graph dynamic based on feature similarity, HybridGNN introduces the additional and distinct dynamism derived from temporal sequence modeling via an RNN. This allows HybridGNN to capture evolving relationships driven by explicit temporal causality (e.g., how the history of one region impacts its connection to another), which is different from a learned graph based solely on current feature interactions.
- Richer Foundation for Propagation: By integrating both the sequence-driven dynamic connections (from the ColaGNN side) and the feature-driven/geographical connections (from the EpiGNN side) into a single adjacency matrix, HybridGNN provides its GNN layers with an unparalleled, multi-faceted view of how regions truly interact and influence each other. This is critical for modeling complex propagation phenomena where both historical patterns and current states dictate connectivity.
- Holistic Pre-GCN Feature Concatenation: HybridGNN strategically prepares its initial node features for GCN propagation by concatenating (rather than summing) Multiscale temporal features, Local transmission risk and Global transmission risk. This holistic concatenation, performed before GCN layers, provides the graph convolutional layers with

an exceptionally rich, multi-faceted initial node representation. By explicitly preserving and processing the distinct contributions of temporal patterns, local risks, and global risks right from the start, the GCNs can learn more nuanced, contextually aware, and disentangled embeddings during message passing. This significantly enhances the GNN's ability to model complex spatio-temporal dependencies with greater precision.

• Deeply Integrated Multi-Perspective Prediction Input: HybridGNN's final prediction layer receives an input that uniquely combines its highly processed spatio-temporal graph output with a distinct, high-level temporal signal from an RNN. This final, deep fusion ensures the model's predictions are exceptionally well-informed, robust, and comprehensive. By leveraging both the deep, context-aware spatio-temporal insights from the GNN (representing the "where" and "what" of propagation) and the explicit, high-level temporal trajectory from the RNN (representing the "when" and "how fast"), HybridGNN can generate more accurate and reliable forecasts for dynamic systems, capturing both the fine-grained interactions and the overarching temporal trends.

7.2 Future Improvements

While HybridGNN's current architecture offers substantial advantages, certain refinements could further enhance its robustness and generalizability, particularly when facing highly volatile or complex system behaviors:

- Advanced Volatility Adaptation: For scenarios characterized by extremely rapid and unpredictable shifts, the model's temporal components could benefit from dynamic weighting mechanisms that can instantly adjust the influence of short-term versus long-term features based on the current observed volatility. This would allow the model to automatically prioritize the most recent information during abrupt changes, preventing older, less relevant patterns from unduly influencing forecasts.
- Deeper Inter-Module Feature Interaction: The current approach to feature fusion, primarily concatenation, could be enhanced. Future work should explore more sophisticated architectural interfaces between modules. This includes designing cross-modal attention mechanisms that enable temporal features to directly modulate spatial aggregation in GCNs, or allowing risk encodings to dynamically refine the weights of connections in the dynamic graph construction process, leading to a more synergistic learning across components.
- Structural Integration of Causal Inference: To move beyond associative learning, a critical architectural evolution involves integrating explicit causal inference modules. This could entail designing specific layers that identify direct causal relationships between nodes or features, subsequently guiding the graph construction or message passing rules to prioritize these causal links. This would not only enhance prediction robustness but also provide invaluable, actionable insights into the underlying drivers of propagation.
- Adaptive Component Contribution in Graph Fusion: The dynamic graph is currently a summation of its parts. A more advanced approach would involve a learnable gating mechanism that dynamically weighs the contribution of each component (e.g., geographical, temporal, external relations) to the final graph structure. This would allow the model to autonomously emphasize the most relevant relational information based on the current context or prediction task, optimizing graph representation on the fly.

By systematically addressing these specific architectural refinements, HybridGNN can evolve into an even more versatile and reliable tool, offering increasingly precise and actionable forecasts that empower decision-makers in the face of diverse and unpredictable real-world challenges.

8 Conclusion and Outlook

EpiGNN and ColaGNN, as graph neural network-based regional epidemic forecasting models, have both significantly improved prediction accuracy and interpretability through innovative architectural designs. EpiGNN focuses on integrating transmission risk and external data, showing superiority in handling dynamic epidemics. ColaGNN, with its dynamic attention mechanism, excels in long-term forecasting and provides insights into propagation dynamics.

Building on this, this paper proposes HybridGNN (EpiCola-GNN), a novel model that combines EpiGNN's strengths in risk encoding and external data integration with ColaGNN's capabilities in long-term forecasting and dynamic attention mechanisms. Experimental results demonstrate that HybridGNN achieves superior prediction performance on multiple datasets (particularly Australia-COVID and US-States), outperforming individual models in short-term accuracy and overall stability, thus validating the effectiveness of our design philosophy in merging the advantages of both models.

Despite the significant progress made by HybridGNN, the field of epidemic forecasting still faces common challenges, such as generalization ability and model robustness on extremely volatile datasets. Future research can further enhance the model's robustness and practicality by introducing mechanisms for temporal decay, enhancing external data robustness, fusing multi-source data, and employing causal modeling. These advancements will provide more reliable support for public health decision-making. Continued research into these advanced GNN models, including our proposed HybridGNN, will keep driving the development of epidemic forecasting.

References

- [1] H. Alabdulrazzaq, et al. On the accuracy of ARIMA based prediction of COVID-19 spread. Results in Physics, 27,104509 (2021).
- [2] M. J. Kane, N. Price, M. Scotch, and P. Rabinowitz. Comparison of ARIMA and Random Forest time series models for prediction of avian influenza H5N1 outbreaks. *BMC Bioinfor*matics, 15,1–9 (2014).
- [3] Z. Wang, P. Chakraborty, S. R. Mekaru, J. S. Brownstein, J. Ye, and N. Ramakrishnan. Dynamic poisson autoregression for influenza-like-illness case count prediction. In: *Proc. of KDD* (2015).
- [4] Michael M. Bronstein, Joan Bruna, Yann LeCun, Arthur Szlam, and Pierre Vandergheynst. 2017. Geometric deep learning: going beyond Euclidean data. *IEEE Signal Processing Magazine*, 34,4(2017),18–42.
- [5] Jie Zhou, Ganqu Cui, Zhengyan Zhang, Cheng Yang, Zhiyuan Liu, and Maosong Sun. 2018. Graph Neural Networks: A Review of Methods and Applications. arXiv preprint arXiv:1812.08434(2018).
- [6] Siva R Venna, Amirhossein Tavanaei, Raju N Gottumukkala, Vijay V Raghavan, Anthony S Maida, and Stephen Nichols. 2018. A novel data-driven model for real-time influenza forecasting. IEEE Access 7 (2018).
- [7] Yuexin Wu, Yiming Yang, Hiroshi Nishiura, and Masaya Saitoh. 2018. Deep Learning for Epidemiological Predictions. In SIGIR. ACM, 1085–1088.
- [8] Lijing Wang, Jiangzhuo Chen, and Madhav Marathe. 2019. DEFSI: Deep Learning Based Epidemic Forecasting with Synthetic Information. In AAAI, Vol. 33. https://doi.org/10. 1609/aaai.v33i01.33019607
- [9] Jung, S., Moon, J., Park, S., Hwang, E.: Self-attention-based deep learning network for regional influenza forecasting. *IEEE JBHI* (2021).
- [10] Yu, B., Yin, H., Zhu, Z.: Spatio-temporal graph convolutional networks: A deep learning framework for traffic forecasting. arXiv preprint arXiv:1709.04875 (2017).
- [11] Shuai Zhang, Hanghang Tong, Jintang Xu, and others. 2019. Graph convolutional networks: a comprehensive review. *Computational Social Networks*, 6(1),1-23.
- [12] Kipf, T.N., Welling, M.: Semi-supervised classification with graph convolutional networks. arXiv preprint arXiv:1609.02907 (2016).
- [13] Xie, F., Zhang, Z., Li, L., Zhou, B., & Tan, Y. (2022, September). EpiGNN: Exploring spatial transmission with graph neural network for regional epidemic forecasting. In *Joint European Conference on Machine Learning and Knowledge Discovery in Databases* (pp. 469-485). Cham: Springer Nature Switzerland.
- [14] Deng, S., Wang, S., Rangwala, H., Wang, L., Ning, Y.: Cola-gnn: Cross-location attention based graph neural networks for long-term ili prediction. In: *Proc. of CIKM* (2020).

- [15] Cho, K., van Merriënboer, B., Gulcehre, C., Bahdanau, D., Bougares, F., Schwenk, H., and Bengio, Y. 2014. Learning Phrase Representations using RNN Encoder–Decoder for Statistical Machine Translation. In Proceedings of the 2014 Conference on Empirical Methods in Natural Language Processing (EMNLP), ACL, Doha, Qatar. https://doi.org/10.3115/v1/D14-1179
- [16] Hochreiter, S. and Schmidhuber, J. 1997. Long short-term memory. Neural Computation 9, 8 (1997), 1735–1780.
- [17] Bahdanau, D., Cho, K., and Bengio, Y. 2014. Neural machine translation by jointly learning to align and translate. arXiv preprint arXiv:1409.0473.
- [18] Ashish Vaswani, Noam Shazeer, Niki Parmar, Jakob Uszkoreit, Llion Jones, Aidan N. Gomez, Łukasz Kaiser, and Illia Polosukhin. 2017. Attention is all you need. Proc. of NeurIPS(2017).
- [19] Sukhbaatar, S., Weston, J., Fergus, R., et al. 2015. End-to-end memory networks. In *Proceedings of the 28th International Conference on Neural Information Processing Systems (NeurIPS)*.
- [20] Johns Hopkins University Center for Systems Science and Engineering. (2021). Daily new COVID-19 confirmed cases in Australia [Data set]. Retrieved from https://github.com/CSSEGISandData/COVID-19 (Accessed: 2025-07-07).
- [21] National Institute of Infectious Diseases, Japan. (2019). Weekly influenza-like-illness (ILI) statistics by prefecture in Japan [Data set]. Retrieved from https://www.niid.go.jp/niid/en/idwr-e.html (Accessed: 2025-07-07).
- [22] U.S. Department of Health & Human Services. (2017). Weekly influenza activity levels by HHS region [Data set]. Retrieved from https://data.cdc.gov/ (Accessed: 2025-07-07).
- [23] Centers for Disease Control and Prevention. (2017). Weekly ILI patient visits by U.S. state [Data set]. Retrieved from https://www.cdc.gov/flu/weekly/ (Accessed: 2025-07-07).
- [24] Kingma, D. P. and Ba, J. 2015. Adam: A Method for Stochastic Optimization. In *Proceedings of the 3rd International Conference on Learning Representations (ICLR)*, abs/1412.6980.